3D UAV Trajectory and Communication Design for Simultaneous Uplink and Downlink Transmission

Meng Hua [ID], *Student Member, IEEE*, Luxi Yang [ID], *Senior Member, IEEE*, Qingqing Wu [ID], *Member, IEEE*, and A. Lee Swindlehurst [ID], *Fellow, IEEE*

Abstract— In this paper, we investigate the unmanned aerial vehicle (UAV)-aided simultaneous uplink and downlink transmission networks, where one UAV acting as a disseminator is connected to multiple access points (AP), and the other UAV acting as a base station (BS) collects data from numerous sensor nodes (SNs). The goal of this paper is to maximize the system throughput by jointly optimizing the 3D UAV trajectory, communication scheduling, and UAV-AP/SN transmit power. We first consider a special case where the UAV-BS and UAV-AP trajectories are pre-determined. Although the resulting problem is an integer and non-convex optimization problem, a globally optimal solution is obtained by applying the polyblock outer approximation (POA) method based on the problem's hidden monotonic structure. Subsequently, for the general case considering the 3D UAV trajectory optimization, an efficient iterative algorithm is proposed to alternately optimize the divided sub-problems based on the successive convex approximation (SCA) technique. Numerical results demonstrate that the proposed design is able to achieve significant system throughput gain over the benchmarks. In addition, the SCA-based method can achieve nearly the same performance as the POA-based method with much lower computational complexity.

Index Terms— UAV, communication design, IoT, 3D trajectory optimization, monotonic optimization.

I. INTRODUCTION

WITH continuing communication device miniaturization and the increased endurance of unmanned aerial vehicles (UAVs), new civilian-use markets are emerging for UAVs beyond military applications, including examples such as emergency search, forest fire detection, cargo transport, etc.

Meng Hua and Luxi Yang are with the School of Information Science and Engineering, Southeast University, Nanjing 210096, China (e-mail: mhua@seu.edu.cn; lxyang@seu.edu.cn).

Qingqing Wu is with the State Key Laboratory of Internet of Things for Smart City, University of Macau, Macao 999078, China, and also with the Department of Electrical and Computer Engineering, University of Macau, Macao 999078, China (e-mail: qingqingwu@um.edu.mo).

A. Lee Swindlehurst is with the Center for Pervasive Communications and Computing, University of California at Irvine, Irvine, CA 92697 USA (e-mail: swindle@uci.edu).

Particularly, UAVs are envisioned as a key component of future wireless network technologies that will expand network coverage and improve system throughput [1]–[3]. Compared with terrestrial base stations (BSs) whose the locations are pre-determined and fixed, UAVs can adaptively control its position to react as needed to requests for on-demand services [4]–[10].

There are two main paradigms for the integration of UAVs in the traditional networks, namely UAV-aided wireless networks and cellular-connected UAV networks [11]–[18]. In the UAV-aided wireless communication scenario, the UAV generally acts as a mobile BS equipped with a communication transceiver to provide seamless wireless services or to collect the data from the ground nodes. UAVs are especially well suited for data collection in sensor networks where the nodes are widely dispersed over a large area [11]–[14]. The sensor nodes (SNs) are typically battery operated, and cannot transmit continuously. Rather than installing dedicated infrastructure, in delay-tolerant applications it is more cost effective to deploy UAVs to visit the SNs and collect the data in a sense-and-carry fashion. In the cellular-connected UAV communication networks, UAVs are regarded as new aerial users that access the cellular network from the sky for communications [15]–[18]. In [19], an in-depth analysis of integration of cellular-connected UAV into the existing wireless networks is provided from the perspectives of multiple metrics. Such UAVs can achieve high data rates with low latency due to the high probability of dominant line-of-sight (LoS) propagation paths with its communication targets.

Despite promising opportunities for UAVs like those mentioned above, some key challenges remain to be addressed in order to effectively use them to realize seamless connectivity and ultra reliable communication in the future. Recently, UAV deployment and trajectory designs for sensing and communications have received great attention [20]–[30]. The deployment of a single UAV was investigated in [20]–[22], especially [22] derived analytical expressions for the optimal UAV altitude that minimizes the system outage probability by using stochastic geometry theory. The deployment of multiple UAVs for either maximizing the coverage area or system throughput was investigated in [23] and [24], respectively. The initial 2D UAV trajectory optimization was studied in [26], where the authors divided the continuous trajectory into multiple discrete segments and solved the discrete problem by convex optimization techniques. Then, 3D trajectory design
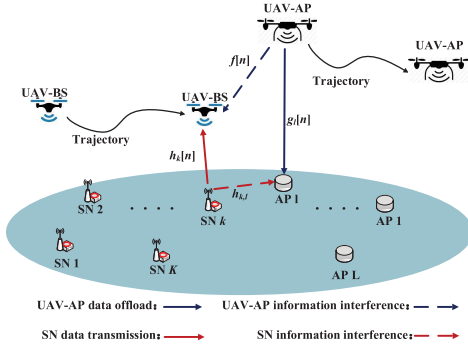
Fig. 1. Coexistence of aerial and cellular-connected UAV networks.

has been studied in [27] and [28]. The goal of [27] was to maximize the minimum average data collection rate from all SNs by optimizing the 3D UAV trajectory under the assumption of Rician fading channels, while the optimal 3D trajectory was obtained by applying monotonic optimization theory in [28]. The problem of multiple UAVs simultaneously serving multiple SNs was first studied in [29] and [30]. In [29], the UAV transmit power and trajectory were optimized to alleviate the interference received by the SNs and maximize the minimum achieved rate from all the SNs. In [30], the authors studied multiple-UAV cooperative secure transmission problem by jointly optimizing the UAV trajectory and transmit power.

While the above work has studied the typical UAV-aided wireless communication network either in the uplink transmission or downlink transmission, question of how to integrate the operation of simultaneous uplink and downlink transmission has not been addressed and remains an open problem. To fill this gap, we study a general heterogeneous network that consists of these two networks. For the downlink transmission network, UAV acts as a disseminator, referred to as UAV-AP, to disseminate data to the ground access point (AP) (Note that the AP is also a type of SNs, we name it as AP to distinguish uplink SNs). For the UAV-BS based network, the UAV acts as a mobile base station (BS), referred to as UAV-BS, to collect data from the uplink SNs. We aim to maximize the sum system throughput, including contributions from both UAV-BS and UAV-AP operations, by jointly optimizing the 3D UAV-BS/UAV-AP trajectory, communication scheduling, and UAV-AP/SN transmit power. We propose an efficient iterative algorithm to address the problem and obtain a locally optimal solution. In addition, for the special case where both UAVs' trajectories are pre-determined, we obtain a globally optimal solution by applying monotonic optimization theory.

As shown in Fig. 1, several challenges must be addressed in order to achieve good performance for the simultaneous uplink and downlink transmission with the help of UAVs. First, in the UAV-AP based network, namely downlink transmission, the AP not only receives the desired signal from the UAV-AP but also suffers from interference from SNs. Second, in the UAV-BS based network, namely uplink transmission, the UAV-BS not only collects desired data from the SNs but also encounters interference from the UAV-AP. To enhance system performance, the UAV-BS/UAV-AP trajectories must

be carefully designed since the UAV location determines its ability to mitigate interference and increase throughput. Furthermore, transmission power of UAV-AP and SN should be jointly optimized to alleviate the whole system interference. Note that this work is different from [31], where a single full-duplex UAV is used to transmit data to the downlink users and receive data from the uplink users simultaneously via a 2D trajectory design. However, self-interference and multiple access delay issues impede its application for the single full-duplex UAV used in delay-sensitive tasks. In this paper, we consider multiple half-duplex UAVs to simultaneously serve downlink users and uplink users, the optimization of altitude and transmission power of UAVs resulting in a heterogeneous networks, which provides additional degrees of freedom for achieving low delay and ultra-reliable communications via a 3D trajectory design. In addition, we propose a novel method to address the resulting problem, and a globally optimal solution is obtained here. It is worth pointing out that work [29] only focuses the case of multiple UAVs serving multiple users in downlink transmission, whereas the uplink transmission is not considered. To the best of our knowledge, this work is first to study simultaneous uplink and downlink transmission with help of multiple UAVs. Our main contributions are summarized as follows.

- We investigate the scenario of simultaneous uplink and downlink transmission with help of multiple UAVs. We focus on maximizing the sum of the UAV-BS and UAV-AP based network throughput subject to the constraints of UAV mobility and SN/UAV-AP transmit power.

- We first study the case that the UAV-BS and UAV-AP trajectories are pre-determined. We aim at maximizing the sum system throughput by jointly optimizing the SN/UAV-AP transmit power and communication scheduling. The resulting optimization problem is a non-convex integer optimization problem, whose solution is difficult to obtain. However, by exploiting the hidden monotonic nature of the problem, we find a globally optimal solution using the polyblock outer approximation (POA) method. Note that although [28] obtains a globally optimal solution to solar-powered UAV systems using POA method, it only focuses on a single UAV in the downlink transmission, we extend it to a more general case with multiple UAVs in the simultaneous uplink and downlink transmission. In addition, we also propose a suboptimal solution based on the successive convex approximation (SCA) technique. Our numerical results show that the SCA-based method can achieve nearly the same system performance as the POA-based method but with much lower computational complexity.

- We then study a more general scenario in which the UAV-BS and UAV-AP trajectories are optimized. Our goal is to maximize the sum system throughput by jointly designing the UAV-BS/UAV-AP trajectories, SN/UAV-AP transmit power, and communication scheduling. The resulting optimization problem is much more challenging to solve. Nevertheless, we decompose the problem into three sub-problems: communication scheduling with fixed transmit power and UAV trajectory sub-problem,

UAV trajectory with fixed transmit power and communication scheduling sub-problem, and transmit power with fixed UAV trajectory and communication scheduling sub-problem. A three-layer iterative algorithm is then proposed to alternately optimize the communication scheduling, UAV trajectory, and transmit power based on the SCA method.

- To demonstrate our designs more clearly, we consider two simulation scenarios. In the first scenario, one UAV-BS collects data from one SN and one UAV-AP transmits its own data to one AP. In the second scenario, the UAV-BS and UAV-AP simultaneously serve multiple SNs and APs. The impact of the weighting factors, UAV trajectory, and transmit power on the system performance are also studied to reveal useful insights. Numerical results show that our proposed scheme achieves significantly higher system throughput compared with other benchmarks.

The rest of the paper is organized as follows. In Section II, we introduce our system model and formulate the system throughput maximization problem. Section III studies the optimal communication design problem. Section IV investigates the joint 3D UAV trajectory and communication design problem. In Section V, numerical results are presented to illustrate the superiority of our scheme. Finally, Section VI concludes the paper.

II. SYSTEM MODEL

We consider an integrated network which consists of a UAV-AP and a UAV-BS based network, as shown in Fig. 1. Without loss of generality, we assume that there are K SNs and L APs, which are in fixed locations. The SN and AP sets are respectively denoted as $\mathcal{K}$ and $\mathcal{L}$. The horizontal coordinates of the kth SN and lth AP are respectively denoted as $\mathbf{w}_{bk}, k \in \mathcal{K}$ and $\mathbf{w}_{ul}, l \in \mathcal{L}$. We assume that the UAVs can adjust their heading as needed. The period T is equally divided into N time slots indexed by $n = 1, \ldots, N$, with duration δ, i.e., $\delta = \frac{T}{N}$. Note that the duration δ should be chosen to be sufficiently small so that the UAV's location can be considered unchanged within each time slot even at the maximum flying speed. As a result, the 3D UAV-AP location at any time slot n is denoted by $\mathbf{w}_u[n] = [\mathbf{q}_u[n] \ H_u[n]]$, where $\mathbf{q}_u[n]$ and $H_u[n]$ denote the horizontal UAV-AP location and altitude, respectively. Similarly, the 3D UAV-BS location at any time slot n is denoted by $\mathbf{w}_b[n] = [\mathbf{q}_b[n] \ H_b[n]]$, where $\mathbf{q}_b[n]$ and $H_u[n]$ denote the horizontal UAV-BS location and altitude, respectively.

For the UAV-to-ground (U2G) channel, ground-to-UAV (G2U) channel, and UAV-to-UAV (U2U) channel, the UAV is likely to establish LoS links for all U2G, G2U, and U2U channels as reported in [11], [32]. To capture the large-scale fading as well as small-scale fading, we model the U2G, G2U, and U2U channels as Rician models [14], [27], [33][1] Thus, the U2G channel coefficient, i.e., UAV-AP to AP l, $\forall l$, at time

slot n can be expressed as

$$\bar{g}_l[n] = \sqrt{\beta_{a,l}[n]} \hat{g}_l[n], \tag{1}$$

where $\beta_{a,l}[n]$ represents its distance-dependent path-loss at time slot n, and $\hat{g}_l[n]$ is a complex-valued random variable that denotes the small-scale fading at time slot n. Specifically, $\beta_{a,l}[n]$ can be written as

$$\beta_{a,l}[n] = \frac{\beta_0}{\left(\|\mathbf{q}_u[n] - \mathbf{w}_{ul}\|^2 + H_u^2[n] \right)^{\kappa_a/2}}, \tag{2}$$

where β_0 denotes the channel power gain at the reference distance of 1 meter, and κ_a denotes the U2G path loss exponent. The small-scale fading, $\hat{g}_l[n]$, can be modeled as below

$$\hat{g}_l[n] = \sqrt{\frac{K_a}{K_a+1}} \tilde{g}_l[n] + \sqrt{\frac{1}{K_a+1}} \tilde{\tilde{g}}_l[n], \tag{3}$$

where $\tilde{g}_l[n]$ denotes the deterministic LoS channel component with $|\tilde{g}_l[n]| = 1$, $\tilde{\tilde{g}}_l[n] \sim \mathcal{CN}(0,1)$ denotes the small fading coefficient, and K_a is the Rician factor for the U2G channel.

Similarly, the channel coefficient from SN k to UAV-BS at time slot n can be expressed as

$$\bar{h}_k[n] = \sqrt{\beta_{s,k}[n]} \hat{h}_k[n], \tag{4}$$

where $\beta_{s,k}[n] = \frac{\beta_0}{\left(\|\mathbf{q}_b[n] - \mathbf{w}_{bk}\|^2 + H_b^2[n] \right)^{\kappa_s/2}}$, $\hat{h}_k[n] = \sqrt{\frac{K_s}{K_s+1}} \tilde{h}_k[n] + \sqrt{\frac{1}{K_s+1}} \tilde{\tilde{h}}_k[n]$, $\left| \tilde{h}_k[n] \right| = 1$, $\tilde{\tilde{h}}_k[n] \sim \mathcal{CN}(0,1)$, and κ_s and K_s denote the G2U path loss exponent and Rician factor, respectively.

Furthermore, the channel coefficient for the U2U channel, i.e., UAV-AP to UAV-BS channel, is given by

$$\bar{f}[n] = \sqrt{\beta_u[n]} \hat{f}[n], \tag{5}$$

where $\beta_u[n] = \frac{\beta_0}{(\|\mathbf{w}_u[n] - \mathbf{w}_b[n]\|)^{\kappa_u/2}}$, $\hat{f}[n] = \sqrt{\frac{K_u}{K_u+1}} \tilde{f}[n] + \sqrt{\frac{1}{K_u+1}} \tilde{\tilde{f}}[n]$, and $\left| \tilde{f}[n] \right| = 1$, $\tilde{\tilde{f}}[n] \sim \mathcal{CN}(0,1)$, and κ_u and K_u denote the U2U path loss exponent and Rician factor, respectively.

Note that the path loss exponents for all the channels depend on the environment. For example, it was shown in [35] that the path loss exponents for U2G/G2U and U2U are 2.32/2.51 and 2.05, respectively, and the results in [36] shown that the path loss exponents for U2G and U2U are 2.13 and 1.92, respectively. Therefore, in the sequel, we set path loss exponents as $\kappa_a = \kappa_s = \kappa_u = 2$ that are consistent with the most existing works [37]–[41]. Although we assume that the path loss exponent is 2, it can be easily extended to the other cases. In addition, we assume that the Rician factors K_a, K_s, and K_u are all invariant over time slot n by considering the following reasons. First, since our scenario is considered in the rural and/or suburban district, i.e., clear airspace, the Rician factor thus can be approximately treated to be independent of the varying UAV locations. Second, especially for the long period flying time T, the most time for UAV is to stay stationary above the ground nodes, and thus can be considered as invariant at most of the time.

---

[1]Although Nakagmi-m also captures the LoS propagation [34], it is so sophisticated for analysis in our considered scenarios. To facilitate the system design, we consider a Rician fading model which is relative simple but still appealing in practice.

In addition, for the ground-to-ground (G2G) channel, we assume that the G2G channel follows Rayleigh fading due to the rich scattering in the environment. Therefore, the channel coefficient from the kth SN to the lth AP can be expressed as

$$\bar{h}_{k,l} = \sqrt{\tilde{h}_{k,l}}\hat{h}_{k,l}, \tag{6}$$

where $\tilde{h}_{k,l} = \frac{\beta_0}{\|\mathbf{w}_{bk} - \mathbf{w}_{ul}\|^\alpha}$ stands for the large-scale path loss, α represents the G2G path loss exponent, and $\hat{h}_{k,l} \sim \mathcal{CN}(0,1)$ denotes the small-scale fading.

To facilitate the system design, we assume the widely used wake-up communication scheduling approach [29], [30], and [40], where the UAV-BS (UAV-AP) can only communicate with at most one SN (AP) in any time slot n. Define the indicator variable $y_k[n], \forall k, n$ and $x_l[n], \forall l, n$ for the UAV-BS and UAV-AP based network, respectively. The UAV-BS serves the kth SN if $y_k[n] = 1$, otherwise, $y_k[n] = 0$. Similarly, if $x_l[n] = 1$, the UAV-AP migrates the data to the lth AP, and no data is transmitted if $x_l[n] = 0$. Thus, we have the following scheduling constraints

$$\sum_{l=1}^{L} x_l[n] \leq 1, \; x_l[n] \in \{0,1\}, \quad \forall l, n, \tag{7}$$

$$\sum_{k=1}^{K} y_k[n] \leq 1, \; y_k[n] \in \{0,1\}, \quad \forall k, n. \tag{8}$$

If the lth AP is awakened to communicate with the UAV-AP at time slot n, the achievable downlink rate of the lth AP is given by

$$\bar{R}_l^u[n] = \log_2\left(1 + \frac{|\bar{g}_l[n]|^2 p^u[n]}{\sum_{k=1}^{K} |\bar{h}_{k,l}|^2 y_k[n] p_k^s[n] + \sigma^2}\right), \tag{9}$$

where $p^u[n]$ and $p_k^s[n]$ respectively denote the UAV-AP and kth SN transmit power at time slot n, and σ^2 represents the noise power at the receiver.

When $y_k[n] = 1$, the uplink transmission rate of SN k is given by

$$\bar{R}_k^s[n] = \log_2\left(1 + \frac{|\bar{h}_k[n]|^2 p_k^s[n]}{\sum_{l=1}^{L} |\bar{f}[n]|^2 x_l[n] p^u[n] + \sigma^2}\right). \tag{10}$$

Obviously, (10) can be simplified as

$$\bar{R}_k^s[n] = \log_2\left(1 + \frac{|\bar{h}_k[n]|^2 p_k^s[n]}{|\bar{f}[n]|^2 p^u[n] + \sigma^2}\right). \tag{11}$$

This is because with (7), if AP l is communicated with UAV-AP at time slot n, namely $x_l[n] = 1$, we have $\sum_{l=1}^{L} |\bar{f}[n]|^2 x_l[n] p^u[n] = |\bar{f}[n]|^2 p^u[n]$; if no AP is activated, the transmission power of UAV-AP $p_u[n]$ must be zero.

Note that since the channels $\{\bar{h}_{k,l}, \bar{h}_k[n], \bar{g}_l[n], \bar{f}[n]\}$ are the random variables, $\bar{R}_k^s[n]$ and $\bar{R}_l^u[n]$ are also the random variables. Additionally, since the probability distribution of $\bar{R}_k^s[n]$ and $\bar{R}_l^u[n]$ are challenging to obtain, we are interested in the expected/average achievable rate, defined as $R_k^s[n] = \mathbb{E}\{\bar{R}_k^s[n]\}$ and $R_l^u[n] = \mathbb{E}\{\bar{R}_l^u[n]\}$. However, the closed-form expressions of $R_k^s[n]$ and $R_l^u[n]$ are unsolvable due to the difficulty of deriving its probability distribution. To address

this issue, we obtain their approximation results based on the following theorem.

Theorem 1: If X is a non-negative positive random variable and Y is a positive random variable, and X and Y are independent, the following approximation result holds

$$\mathbb{E}\left\{\log_2\left(1 + \frac{X}{Y}\right)\right\} \approx \log_2\left(1 + \frac{\mathbb{E}\{X\}}{\mathbb{E}\{Y\}}\right). \tag{12}$$

Proof: Please refer to Appendix A. ∎

Based on Theorem 1, we can, respectively, recast $R_k^s[n]$ and $R_l^u[n]$ as

$$
\begin{aligned}
R_k^s[n] &\approx \log_2\left(1 + \frac{\mathbb{E}\left\{|\bar{h}_k[n]|^2\right\} p_k^s[n]}{\mathbb{E}\left\{|\bar{f}[n]|^2\right\} p^u[n] + \sigma^2}\right) \\
&\triangleq \log_2\left(1 + \frac{h_k[n] p_k^s[n]}{f[n] p^u[n] + \sigma^2}\right)
\end{aligned} \tag{13}
$$

and

$$
\begin{aligned}
R_l^u[n] &\approx \log_2\left(1 + \frac{\mathbb{E}\left\{|\bar{g}_l[n]|^2\right\} p^u[n]}{\sum_{k=1}^{K} \mathbb{E}\left\{|\bar{h}_{k,l}|^2\right\} y_k[n] p_k^s[n] + \sigma^2}\right) \\
&\triangleq \log_2\left(1 + \frac{g_l[n] p^u[n]}{\sum_{k=1}^{K} \tilde{h}_{k,l} y_k[n] p_k^s[n] + \sigma^2}\right),
\end{aligned} \tag{14}
$$

where $h_k[n] = \beta_{s,k}[n], g_l[n] = \beta_{a,l}[n]$, and $f[n] = \beta_u[n]$. The accuracy for the approximation results of $R_k^s[n]$ and $R_l^u[n]$ will be evaluated later in Section V.

In this paper, we focus on the joint design of the UAV trajectory, communication scheduling, and transmit power to maximize the integrated network throughput, i.e., the sum throughput of the UAV-BS and UAV-AP based networks. Define sets $A = \{x_l[n], y_k[n], \forall l, k, n\}$, $P = \{p^u[n], p_k^s[n], \forall k, n\}$, and $Q = \{\mathbf{w}_u[n], \mathbf{w}_b[n], \forall n\}$. Then, the problem can be formulated as[2]

$$\max_{A,P,Q} \beta_1 \sum_{n=1}^{N}\sum_{k=1}^{K} y_k[n]\log_2\left(1 + \frac{h_k[n] p_k^s[n]}{f[n] p^u[n] + \sigma^2}\right)$$

$$+ \beta_2 \sum_{n=1}^{N}\sum_{l=1}^{L} x_l[n]\log_2$$

$$\times \left(1 + \frac{g_l[n] p^u[n]}{\sum_{k=1}^{K} \tilde{h}_{k,l} y_k[n] p_k^s[n] + \sigma^2}\right) \tag{15a}$$

$$\text{s.t.} \; \sum_{l=1}^{L} x_l[n] \leq 1, \; x_l[n] \in \{0,1\}, \quad \forall l, n, \tag{15b}$$

$$\sum_{k=1}^{K} y_k[n] \leq 1, \; y_k[n] \in \{0,1\}, \quad \forall k, n, \tag{15c}$$

$$0 \leq p^u[n] \leq p_{\max}^u, \quad \forall n, \tag{15d}$$

$$0 \leq p_k^s[n] \leq p_{\max}^s, \quad \forall k, n, \tag{15e}$$

$$\|H_i[n] - H_i[n-1]\| \leq V_z\delta, \forall n, i \in \{b, u\}, \tag{15f}$$

$$H_{\min} \leq H_i[n] \leq H_{\max}, \forall n, i \in \{b, u\}, \tag{15g}$$

$$H_i[0] = H_{I_i}, H_i[N] = H_{F_i}, i \in \{b, u\}, \tag{15h}$$

$$\|\mathbf{q}_i[n] - \mathbf{q}_i[n-1]\| \leq V_{xy}\delta, \forall n, i \in \{b, u\}, \tag{15i}$$

---

[2]The formulated problem can be easily extended to the case where the different links have different priorities by setting different weighting factors on the different links in the objective function.

$$\mathbf{q}_i\,[0] = \mathbf{q}_{I_i}, \mathbf{q}_i\,[N] = \mathbf{q}_{F_i}, i \in \{b,u\}, \tag{15j}$$

$$\|\mathbf{q}_b\,[n] - \mathbf{q}_u\,[n-1]\|^2$$
$$+ \|H_b\,[n] - H_u\,[n]\|^2 \geq d_{\min}^2, \forall n, \tag{15k}$$

where β_1 and β_2 are the weighting factors. Equations (15d) and (15e) represent the transmit power constraints, with $p_{\max}^u$ and $p_{\max}^s$ denoting the maximum power limits at the UAV-AP and SNs, respectively. Equations (15f)-(15j) denotes the UAV trajectory constraints, where V_z and V_{xy} respectively denote the maximum UAV vertical and horizontal speed, H_{I_i} and $\mathbf{q}_{I_i}$ represent the initial location for UAV i, H_{F_i} and $\mathbf{q}_{F_i}$ represents the final location for UAV i. Finally, (15k) denotes the collision avoidance constraint between the two UAVs with a minimum safety distance $d_{\min}$.

III. GLOBALLY OPTIMAL COMMUNICATION DESIGN

In this section, we obtain the globally optimal solution to (15) for the particular case when the two UAV trajectories are pre-determined. In practice, for a large number of UAV applications, the flight paths are fixed, e.g., the UAV flies in a circular path along the cell edge to serve the cell-edge users, or the UAV flies in a straight line to communicate with the ground users [38], [42]. As a result, (15) is simplified as

$$\max_{A,P} \beta_1 \sum_{n=1}^{N} \sum_{k=1}^{K} y_k\,[n]\log_2\left(1 + \frac{h_k\,[n]\,p_k^s\,[n]}{f\,[n]\,p^u\,[n]+\sigma^2}\right)$$

$$+ \beta_2 \sum_{n=1}^{N} \sum_{l=1}^{L} x_l[n]\log_2$$

$$\times \left(1 + \frac{g_l[n]p^u\,[n]}{\sum_{k=1}^{K} \tilde{h}_{k,l}y_k\,[n]\,p_k^s\,[n]+\sigma^2}\right) \tag{16a}$$

$$\text{s.t. (15b)-(15e).} \tag{16b}$$

Problem (16) is difficult to solve due to the coupled power and communication scheduling in (16a) and the binary variables in (15b) and (15c). However, we show how to optimally solve (16) by using monotonic optimization theory [43], [44]. First, it is observed that $y_k[n]$ and $x_l[n]$ in (16a) can be moved into the numerator of the logarithm terms since $y_k[n] = 1$ for at most one k ($x_l[n] = 1$ for at most one l). Either way, the terms where $y_k[n] = 0$ and $x_l[n] = 0$ do not contribute to the objective valuable. Defining $\tilde{p}_l^u\,[n] = p^u\,[n]\,x_l\,[n]$ for all l, $\tilde{p}_k^s\,[n] = p_k^s\,[n]\,y_k\,[n]$ for all k, and $\tilde{P} = \{\tilde{p}^u\,[n], \tilde{p}_k^s\,[n], \forall k, n\}$, we formulate the following problem:

$$\max_{\tilde{P}} \beta_1 \sum_{n=1}^{N} \sum_{k=1}^{K} \log_2$$

$$\times \left(1 + \frac{h_k\,[n]\,\tilde{p}_k^s\,[n]}{M\sum_{i\neq k}^{K} \tilde{p}_i^s\,[n]+\sum_{l=1}^{L} f\,[n]\,\tilde{p}_l^u\,[n]+\sigma^2}\right)$$

$$+ \beta_2 \sum_{n=1}^{N} \sum_{l=1}^{L} \log_2$$

$$\times \left(1 + \frac{g_l[n]\tilde{p}_l^u\,[n]}{M\sum_{i\neq l}^{L} \tilde{p}_i^u\,[n]+\sum_{k=1}^{K} \tilde{h}_{k,l}\tilde{p}_k^s\,[n]+\sigma^2}\right) \tag{17a}$$

$$\text{s.t.}\ \tilde{P} \in \mathcal{P}, \tag{17b}$$

where $\mathcal{P} = \left\{\tilde{P}|0 \leq \tilde{p}_l^u\,[n] \leq p_{\max}^u, 0 \leq \tilde{p}_k^s\,[n] \leq p_{\max}^s, \forall k, l, n\right\}$, and M is a sufficiently large penalty factor.

Theorem 2: Problem (17) is equivalent to (16).

Proof: Please refer to Appendix B. ∎

There is no standard method to obtain the optimal solution to (17) due to the coupled transmit power in the objective function. However, by exploiting the hidden monotonicity in the problem, we obtain the optimal solution to problem (17) by following two steps. We first transform problem (17) into an equivalent canonical monotonic optimization formulation. Then, we apply a sequence of ployblocks to approach the optimal vertex using POA method. Specifically, by introducing the auxiliary variables $\chi_k[n]$ and $\bar{\chi}_l[n]$, problem (17) can be equivalently written as

$$\max_{\chi_k[n], \bar{\chi}_l[n]} \beta_1 \sum_{n=1}^{N} \sum_{k=1}^{K} \log_2\left(1 + \chi_k\,[n]\right)$$

$$+ \beta_2 \sum_{n=1}^{N} \sum_{l=1}^{L} \log_2\left(1 + \bar{\chi}_l\,[n]\right) \tag{18a}$$

$$\text{s.t.}\ \left(\boldsymbol{\chi}_k\,[n], \bar{\boldsymbol{\chi}}_l\,[n]\right) \in \mathcal{G}, \tag{18b}$$

where $\boldsymbol{\chi}_k\,[n]$ and $\bar{\boldsymbol{\chi}}_l\,[n]$ are the collections of $\chi_k[n]$ and $\bar{\chi}_l[n]$, respectively, and the normal set $\mathcal{G}$ is defined in (19), as shown at the bottom of the page. Note that the signal-to-interference-plus-noise-ratio (SINR) for the UAV-BS and UAV-AP based networks must be non-negative. Therefore, both $\chi_k[n]$ and $\bar{\chi}_l[n]$ must be no smaller than than zero, i.e., $\mathcal{H} = \{(\chi_k[n], \bar{\chi}_l[n]) | \chi_k[n] \geq 0, \bar{\chi}_l[n] \geq 0, \forall k, l, n\}$. It can be seen that the objective function in (18) is an increasing function with $\chi_k[n]$ and $\bar{\chi}_l[n]$. In addition, the power allocation $\tilde{p}_l^u[n]$ and $\tilde{p}_k^s[n]$ in the normal $\mathcal{G}$ in (19) can be optimally obtained when $\chi_k[n]$ and $\bar{\chi}_l[n]$ are fixed (see (20) for more details). Therefore, (18) is in the canonical form of a monotonic optimization problem, and the optimal solution can be obtained by searching the upper boundary of the feasible set using the POA method, which is summarized in Algorithm 1 [43], [44].

To explain Algorithm 1 more clearly, we provide a simple case that includes two optimization variables $\chi[n]$ and $\bar{\chi}[n]$ as shown in Fig. 2. In the initial stage of Algorithm 1, we set

$$\mathcal{G} = \left\{(\chi_k\,[n], \bar{\chi}_l\,[n])\,|\chi_k\,[n] \leq \frac{h_k\,[n]\,\tilde{p}_k^s\,[n]}{M\sum_{i\neq k}^{K} \tilde{p}_i^s\,[n]+\sum_{l=1}^{L} f\,[n]\,\tilde{p}_l^u\,[n]+\sigma^2},\right.$$

$$\left.\bar{\chi}_l\,[n] \leq \frac{g_l[n]\tilde{p}_l^u\,[n]}{M\sum_{i\neq l}^{L} \tilde{p}_i^u\,[n]+\sum_{k=1}^{K} \tilde{h}_{k,l}\tilde{p}_k^s\,[n]+\sigma^2}, \forall l, k, n, \tilde{P} \in P\right\} \tag{19}$$

Algorithm 1 Polyblock Outer Approximation (POA) Based Method

1: **Initialize** polyblock $\mathcal{S}^1$ with vertex $\boldsymbol{v}^1 = (\chi_k^1[n], \bar{\chi}_l^1[n])$, where $\chi_k^1[n] = \frac{h_k[n]p_{\max}^s}{\sigma^2}$ and $\bar{\chi}_l^1[n] = \frac{g_l[n]p_{\max}^u}{\sigma^2}$ for $\forall k, l, n$; $\mathcal{T}^1 = \{\boldsymbol{v}^1\}$, maximum tolerance $\epsilon = 10^{-2}$, and iterative index $t = 1$.
2: **Repeat**
3:    Compute the projection of $\mathbf{v}^t$ on the upper boundary of $\mathcal{G}$, denoted as $\boldsymbol{\pi}^{\mathcal{G}}(\mathbf{v}^t)$, via Algorithm 2.
4:    With $\boldsymbol{\pi}^{\mathcal{G}}(\mathbf{v}^t)$, generate M new vertices $\{\tilde{\mathbf{v}}_1^t, \ldots, \tilde{\mathbf{v}}_M^t\}$, where $\tilde{\mathbf{v}}_i^t = \mathbf{v}^t - (v_i^t - \pi_i^{\mathcal{G}}(\mathbf{v}^t))\,\mathbf{e}_i$ for $i = 1, \ldots, M$.
5:    Construct a smaller polyblock $\mathcal{S}^{t+1}$ with vertex set $\mathcal{T}^{t+1}$ by replacing $\mathbf{v}^t$ in $\mathcal{T}^t$ with M new vertices $\{\tilde{\mathbf{v}}_1^t, \ldots, \tilde{\mathbf{v}}_M^t\}$.
6:    Find $\mathbf{v}^{t+1}$ as the candidate vertex that maximizes the objective function of problem (18) over set $\mathcal{T}^{t+1} \cap \mathcal{H}$.
7:    $t = t + 1$.
8: **Until** $\max\limits_i \left\{ \frac{\|\mathbf{v}_i^t - \pi_i^{\mathcal{G}}(\mathbf{v}^t)\|}{\|\mathbf{v}_i^t\|} \right\} \le \epsilon$.
9: Output optimal transmit power $\{\tilde{p}_k^{s,*}[n]\}$ and $\{\tilde{p}_l^{u,*}[n]\}$ by computing $\boldsymbol{\pi}^{\mathcal{G}}(\mathbf{v}^t)$ in Algorithm 2.

Algorithm 2 Bisection Search to Compute $\boldsymbol{\pi}^{\mathcal{G}}(\mathbf{v}^t)$

1: **Initialize:** $\lambda_{\min} = 0$, $\lambda_{\max} = 1$, $\epsilon = 10^{-2}$.
2: **Repeat**
3:    Compute $\lambda = \frac{\lambda_{\min} + \lambda_{\max}}{2}$
4:    Check the feasibility of problem (20), i.e., $\lambda \mathbf{v}^t \in \mathcal{G}$. If yes, let $\lambda_{\min} = \lambda$, otherwise, let $\lambda_{\max} = \lambda$.
5: **Until** $\lambda_{\max} - \lambda_{\min} \le \epsilon$
6: Output $\lambda = \lambda_{\min}$ and $\pi^G(\mathbf{v}^t) = \lambda \mathbf{v}^t$. The optimal power allocation $\{\tilde{p}_k^{s,*}[n]\}$ and $\{\tilde{p}_l^{u,*}[n]\}$ are obtained by solving problem (20) for $\lambda = \lambda_{\min}$.
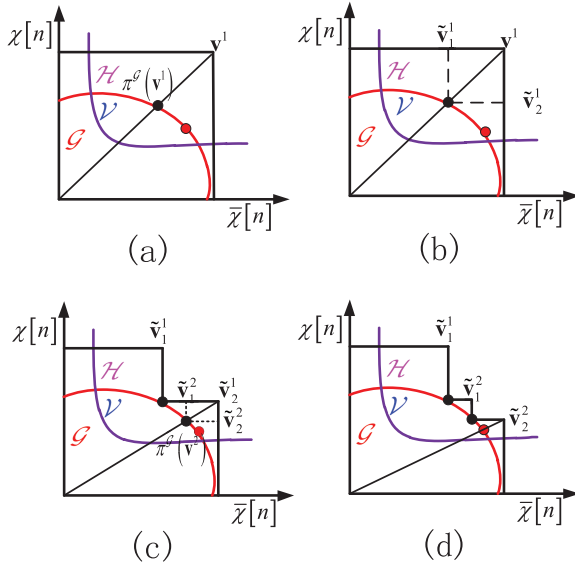

Fig. 2. Illustration of Algorithm 1, where the red circle denotes the optimal point on the upper boundary of the feasible set $\mathcal{V} = \mathcal{G} \cap \mathcal{H}$.

$\chi_k^1[n] = \frac{h_k[n]p_{\max}^s}{\sigma^2}$ and $\bar{\chi}_l^1[n] = \frac{g_l[n]p_{\max}^u}{\sigma^2}$, $\forall k, l, n$, and define vertex $\mathbf{v}^1$ as $\mathbf{v}^1 = (\chi_k^1[n], \bar{\chi}_l^1[n])$. It is clear that polyblock $\mathcal{S}^1$ is a box $[\mathbf{0}\ \mathbf{v}^1]$ comprising the feasible set $\mathcal{V} = \mathcal{G} \cap \mathcal{H}$. In step 3, we calculate the projection of vertex $\mathbf{v}^1$ onto set $\mathcal{G}$, i.e., $\boldsymbol{\pi}^{\mathcal{G}}(\mathbf{v}^1)$ (see Fig. 2 (a)). In step 4, based on vertex $\mathbf{v}^1$ and $\boldsymbol{\pi}^{\mathcal{G}}(\mathbf{v}^1)$, we generate $M = (K + L)N$ new vertices, denoted as $\{\tilde{\mathbf{v}}_1^1, \ldots, \tilde{\mathbf{v}}_M^1\}$, where $\tilde{\mathbf{v}}_i^1 = \mathbf{v}^1 - (v_i^1 - \pi_i^{\mathcal{G}}(\mathbf{v}^1))\,\mathbf{e}_i$ (see Fig. 2 (b)). Here, v_i^1 is the ith element of $\mathbf{v}^1$, $\pi_i^{\mathcal{G}}(\mathbf{v}^1)$ is the ith element of $\boldsymbol{\pi}^{\mathcal{G}}(\mathbf{v}^1)$, and $\mathbf{e}_i$ denotes the ith column of the identity matrix. In step 5, we shrink the polyblock $\mathcal{S}^1$, denoted as polyblock $\mathcal{S}^2$, by replacing $\mathbf{v}^1$ with the new vertices set $\mathcal{T}^2$, i.e., $\mathcal{T}^2 = (\mathcal{T}^1 - \tilde{\mathbf{v}}^1) \cup \{\tilde{\mathbf{v}}_1^1, \ldots, \tilde{\mathbf{v}}_M^1\}$ (see Fig. 2 (c)). It can be observed that polyblock $\mathcal{S}^2$ still contains the feasible

set $\mathcal{V}$ but is smaller than polyblock $\mathcal{S}^1$. Then, we choose the vertex from $\mathcal{T}^2 \cap H$ that maximizes the objective function of problem (18) (see $\tilde{\mathbf{v}}_2^1$ in Fig. 2 (c)). Similarly, we repeat the above procedures to find a smaller and tighter polyblock that satisfies $\mathcal{S}^1 \supset \mathcal{S}^2 \supset \cdots \supset \mathcal{V}$ (see Fig. 2 (d)). Therefore, Algorithm 1 will finally approach the optimal solution when $\max\limits_i \left\{ \frac{\|\mathbf{v}_i^t - \pi_i^{\mathcal{G}}(\mathbf{v}^t)\|}{\|\mathbf{v}_i^t\|} \right\} \le \epsilon$.

Find solutions : $\{\tilde{p}_k^s[n], \tilde{p}_l^u[n]\}$

$$\text{s.t.} \quad \lambda \chi_k[n] \le \frac{h_k[n]\tilde{p}_k^s[n]}{M\sum_{i \ne k}^K \tilde{p}_i^s[n] + \sum_{l=1}^L f[n]\tilde{p}_l^u[n] + \sigma^2}, \tag{20a}$$

$$\lambda \bar{\chi}_l[n] \le \frac{g_l[n]\tilde{p}_l^u[n]}{M\sum_{i \ne l}^L \tilde{p}_i^u[n] + \sum_{k=1}^K \tilde{h}_{k,l}\tilde{p}_k^s[n] + \sigma^2}. \tag{20b}$$

$$0 \le \tilde{p}_l^u[n] \le p_{\max}^u, \quad \forall n, \tag{20c}$$

$$0 \le \tilde{p}_k^s[n] \le p_{\max}^s, \quad \forall k, n. \tag{20d}$$

Following [43, Proposition 6], the value $\boldsymbol{\pi}^{\mathcal{G}}(\mathbf{v}^t)$ in step 3 of Algorithm 1 can be calculated as follows: $\boldsymbol{\pi}^{\mathcal{G}}(\mathbf{v}^t) = \lambda \mathbf{v}^t$, where $\lambda = \max\{a|a\mathbf{v}^t \in \mathcal{G}\}$, and the details are summarized in Algorithm 2. Note that (20) in Algorithm 2 can be recast as a linear optimization problem by transforming the fractional constraints (20a) and (20b) into linear forms, and thus can be optimally solved. Then, we can recover the optimal transmit power for (16) using the following steps: if $\tilde{p}_k^s[n] > 0$, $y_k[n] = 1$ and $p_k^s[n] = \tilde{p}_k^s[n]$; and if $\tilde{p}_k^s[n] = 0$, $y_k[n] = 0$ and $p_k^s[n] = 0$. Similar to $p^u[n]$, if $\tilde{p}_l^u[n] > 0$, $x_l[n] = 1$ and $p^u[n] = \tilde{p}_l^u[n]$.

A. Optimality and Complexity Analysis

The optimality analysis of Algorithm 1 is given as follows: In every iteration in step 4 of Algorithm 1, we can generate a subsequence thought as the "off-springs" through a series of projections. Therefore, an infinite length of sequences can be obtained as the number of iteration increases. Clearly, we always have the sequence: $\mathbf{v}^1 \succeq \mathbf{v}^2 \succeq \cdots \succeq \mathbf{v}^t \succeq \mathbf{v}^{t+1} \cdots \succeq \mathbf{0}$. Hence, $\lim\limits_{t \to \infty} \|\mathbf{v}^t - \mathbf{v}^{t+1}\| \to 0$. We assume that $\mathbf{v}^{t+1}$ is a vector picking from the "off-springs" subsequence, i.e., subsequence $\{\tilde{\mathbf{v}}_1^t, \ldots, \tilde{\mathbf{v}}_M^t\}$, obtained from $\mathbf{v}^t$. Without loss of generality, we assume that $\mathbf{v}^{t+1} = \tilde{\mathbf{v}}_m^t$. As

$t \to \infty$, we have $\lim\limits_{t\to\infty} \left\| \mathbf{v}^t - \mathbf{v}^{t+1} \right\| = \lim\limits_{t\to\infty} \left\| \mathbf{v}^t - \tilde{\mathbf{v}}_m^t \right\| \overset{(a)}{=} v_m^t - \boldsymbol{\pi}_m^G(\mathbf{v}^t) \to 0$, where (a) holds since $\tilde{\mathbf{v}}_m^t = \mathbf{v}^t - \left(v_m^t - \boldsymbol{\pi}_m^G(\mathbf{v}^t) \right) \mathbf{e}_m$. In addition, since $\boldsymbol{\pi}_m^G(\mathbf{v}^t) = \lambda v_m^t$, we have $\left| v_m^t - \lambda v_m^t \right| \to 0$, which implies $\lambda \to 1$. We thus have $\lim\limits_{t\to\infty} \left\| \mathbf{v}^t - \boldsymbol{\pi}^G(\mathbf{v}^t) \right\| = \lim\limits_{t\to\infty} \left\| \mathbf{v}^t - \lambda \mathbf{v}^t \right\| \to 0$. Recall that the optimal solution lies on the upper boundary of $\mathcal{G}$, and $\mathbf{v}^t$ is a maximizer over the above sequence, the globally optimal solution is thus obtained. The reader can also refer to [Theorem 1, [43]] for more details.

The computational complexity of Algorithm 1 is analyzed as follows: The complexity of Algorithm 1 mainly depends on the calculation of $\boldsymbol{\pi}^G(\mathbf{v}^t)$ in step 3, the calculation of picking the optimal vertex from the sequences that maximizes the objective value in step 6, and the total number of iterations required to converge. In the tth iteration, the complexity of computing $\boldsymbol{\pi}^G(\mathbf{v}^t)$ by using Algorithm 2 is $\mathcal{O}\left(\log_2 \left(\frac{\lambda_{\max} - \lambda_{\min}}{\epsilon} \right) \sqrt{M} \right)$, where $\log_2 \left(\frac{\lambda_{\max} - \lambda_{\min}}{\epsilon} \right)$ is the number of iterations required for reaching convergence by using the bisection method, and $\sqrt{M}$ is the complexity of solving linear optimization problem (20) at each iteration in step 4 in Algorithm 2. For each vertex, the complexity for computing the objective function in (18) is $\mathcal{O}(M)$, thus the total complexity of step 6 is $\mathcal{O}\left((tM - (t-1))M\right)$, where $tM - (t-1)$ is the number of vertices. It was shown in [45] that the total number of iterations, denoted as T_c, required for convergence grows exponentially with M, i.e., $T_c = \mathcal{O}\left(2^M\right)$. Therefore, the total complexity of Algorithm 1 is $\mathcal{O}\left(T_c \log_2 \left(\frac{\lambda_{\max} - \lambda_{\min}}{\epsilon} \right) \sqrt{M} + \frac{(M + T_c M - T_c + 1)T_c}{2} \right)$.

We note that although a globally optimal solution for (16) using the POA method is obtained, the computational complexity grows exponentially with the number of variables M. To address this issue, a lower-complexity SCA-based method is discussed in the next section.

IV. JOINT 3D TRAJECTORY AND COMMUNICATION DESIGN OPTIMIZATION

In this section, we investigate the joint 3D trajectory and communication design optimization for maximizing the system throughput using the low-complexity SCA method. Problem (15) is a mixed integer and non-convex optimization problem due to the objective function (15a), constraints (15b), (15c), and (15k). We decompose problem (15) into three sub-problems, and then optimize each sub-problem in an iterative way. Specifically, the three sub-problems are the communication scheduling optimization with fixed transmit power and 3D UAV trajectory; the 3D UAV trajectory optimization with fixed transmit power and communication scheduling; the transmit power optimization with fixed communication scheduling and 3D UAV trajectory. First, we relax the integer communication scheduling constraints (15b) and (15c) into continuous constraints as

$$\sum_{l=1}^{L} x_l[n] \le 1, \ 0 \le x_l[n] \le 1, \forall l, n, \tag{21}$$

$$\sum_{k=1}^{K} y_k[n] \le 1, \ 0 \le y_k[n] \le 1, \forall k, n, \tag{22}$$

A. Communication Scheduling Optimization With Fixed Transmit Power and Trajectory

For any given Q and P, the communication scheduling sub-problem is given by

$$\max_{y_k[n], x_l[n]} \beta_1 \sum_{n=1}^{N} \sum_{k=1}^{K} y_k[n] \log_2 \left(1 + \frac{h_k[n] p_k^s[n]}{f[n] p^u[n] + \sigma^2} \right)$$

$$+ \beta_2 \sum_{n=1}^{N} \sum_{l=1}^{L} x_l[n] \log_2$$

$$\times \left(1 + \frac{g_l[n] p^u[n]}{\sum\limits_{k=1}^{K} \tilde{h}_{k,l} y_k[n] p_k^s[n] + \sigma^2} \right) \tag{23a}$$

$$\text{s.t. (21), (22).} \tag{23b}$$

As can be seen, (23a) is convex but not concave w.r.t to $y_k[n]$, which makes problem (23) non-convex. To tackle it, we apply the SCA method [46]. Specifically, for any feasible point $y_k^r[n]$ in the rth iteration, we have

$$R_l^u[n] \ge \log_2 \left(1 + \frac{g_l[n] p^u[n]}{\sum_{k=1}^{K} \tilde{h}_{k,l} y_k^r[n] p_k^s[n] + \sigma^2} \right)$$

$$- \sum_{k=1}^{K} A_k^l \left(y_k[n] - y_k^r[n] \right) \overset{\triangle}{=} \varphi^{lb}(R_l^u[n]), \tag{24}$$

where

$$A_k^l = \frac{g_l[n] p^u[n] \tilde{h}_{k,l} p_k^s[n] \log_2 e}{\left(\sum\limits_{k=1}^{K} \tilde{h}_{k,l} y_k^r[n] p_k^s[n] + \sigma^2 \right) \left(\sum\limits_{k=1}^{K} \tilde{h}_{k,l} y_k^r[n] p_k^s[n] + \sigma^2 + g_l[n] p^u[n] \right)}.$$

Obviously, $\varphi^{lb}(R_l^u[n])$ is linear with $y_k[n]$, which is convex. Therefore, the value $y_k^{r+1}[n]$ in the $r+1$th iteration can be achieved by solving the following convex problem:

$$\max_{y_k[n], x_l[n]} \beta_1 \sum_{n=1}^{N} \sum_{k=1}^{K} y_k[n] \log_2 \left(1 + \frac{h_k[n] p_k^s[n]}{f[n] p^u[n] + \sigma^2} \right)$$

$$+ \beta_2 \sum_{n=1}^{N} \sum_{l=1}^{L} x_l[n] \varphi^{lb}(R_l^u[n]) \tag{25a}$$

$$\text{s.t. (21), (22).}$$

By successively updating the $y_k^r[n]$, a locally optimal solution can be found.

B. 3D UAV Trajectory Optimization With Fixed Transmit Power and Communication Scheduling

For any given A and P, the 3D trajectory problem is given by

$$\max_{Q} \beta_1 \sum_{n=1}^{N} \sum_{k=1}^{K} y_k[n] \log_2 \left(1 + \frac{h_k[n] p_k^s[n]}{f[n] p^u[n] + \sigma^2} \right)$$

$$+ \beta_2 \sum_{n=1}^{N} \sum_{l=1}^{L} x_l[n] \log_2$$

$$\times \left(1 + \frac{g_l[n] p^u[n]}{\sum_{k=1}^{K} \tilde{h}_{k,l} y_k[n] p_k^s[n] + \sigma^2} \right) \tag{26a}$$

$$\text{s.t. (15f)-(15k).} \tag{26b}$$

Problem (26) is non-convex due to the non-convex objective function (26a) and non-convex constraint (15k). Let $\psi\left(R_l^u\left[n\right]\right)$ be the first order Taylor expansion of $R_l^u[n]$ at the feasible point $Z_l^{u,r}[n] \triangleq \left\|\mathbf{q}_u^r\left[n\right] - \mathbf{w}_{ul}\right\|^2 + H_u^r[n]^2$ in the rth iteration, which is given by

$$
\begin{aligned}
&\psi\left(R_l^u\left[n\right]\right) \\
&= \log_2\left(1 + \frac{S_{1,l}\left[n\right]}{\left\|\mathbf{q}_u^r\left[n\right] - \mathbf{w}_{ul}\right\|^2 + H_u^r[n]^2}\right) - S_{2,l}\left[n\right] \\
&\quad \times \left(\left\|\mathbf{q}_u[n] - \mathbf{w}_{ul}\right\|^2 + H_u[n]^2 - \left\|\mathbf{q}_u^r[n] - \mathbf{w}_{ul}\right\|^2 - H_u^r[n]^2\right),
\end{aligned}
\tag{27}
$$

where $S_{1,l}\left[n\right] = \frac{p^u[n]\beta_0}{\sum_{k=1}^K \tilde{h}_{k,l} y_k[n] p_k^s[n] + \sigma^2}$ and $S_{2,l}\left[n\right] = \frac{S_{1,l}[n]}{Z_l^{u,r}[n]\left(Z_l^{u,r}[n] + S_{1,l}[n]\right)}$. Equation (27) is concave w.r.t the UAV trajectory variable Q. In addition, $R_k^s\left[n\right]$ in (26a) can be rewritten as

$$
R_k^s\left[n\right] = \hat{R}_k^s\left[n\right] - \log\left(\frac{\beta_0 p^u\left[n\right]}{\left\|\mathbf{w}_u\left[n\right] - \mathbf{w}_b\left[n\right]\right\|^2} + \sigma^2\right), \tag{28}
$$

where

$$
\begin{aligned}
\hat{R}_k^s\left[n\right] = \log\Bigg(&\frac{\beta_0 p^u\left[n\right]}{\left\|\mathbf{w}_u\left[n\right] - \mathbf{w}_b\left[n\right]\right\|^2} \\
&+ \frac{\beta_0 p_k^s\left[n\right]}{\left\|\mathbf{q}_b\left[n\right] - \mathbf{w}_{bk}\right\|^2 + H_b[n]^2} + \sigma^2\Bigg)
\end{aligned}
\tag{29}
$$

By introducing the slack variables $\Upsilon\left[n\right]$, (28) can be recast as

$$
R_k^s\left[n\right] = \hat{R}_k^s\left[n\right] - \log\left(\frac{\beta_0 p^u\left[n\right]}{\Upsilon\left[n\right]} + \sigma^2\right), \tag{30}
$$

with the additional constraints

$$
0 < \Upsilon\left[n\right] \le \left\|\mathbf{w}_u\left[n\right] - \mathbf{w}_b\left[n\right]\right\|^2, \forall n. \tag{31}
$$

We can see that the second term $\log\left(\frac{\beta_0 p^u[n]}{\Upsilon[n]} + \sigma^2\right)$ in (30) is convex w.r.t. $\Upsilon\left[n\right]$. However, the new constraint (31) is non-convex. Let $\psi\left(\Upsilon\left[n\right]\right)$ be the first order Taylor expansion of $\left\|\mathbf{w}_u\left[n\right] - \mathbf{w}_b\left[n\right]\right\|^2$ at the feasible point $\mathbf{w}_u^r\left[n\right] = \left[\mathbf{q}_u^r\left[n\right] \; H_u^r\left[n\right]\right], \mathbf{w}_b^r\left[n\right] = \left[\mathbf{q}_b^r\left[n\right] \; H_b^r\left[n\right]\right]$ in the rth iteration. Then, we have

$$
\begin{aligned}
\psi\left(\Upsilon\left[n\right]\right) = &\left\|\mathbf{w}_u^r\left[n\right] - \mathbf{w}_b^r\left[n\right]\right\|^2 + 2\left(\mathbf{w}_u^r\left[n\right] - \mathbf{w}_b^r\left[n\right]\right) \\
&\times \left(\mathbf{w}_u\left[n\right] - \mathbf{w}_u^r\left[n\right]\right)^T \\
&- 2\left(\mathbf{w}_u^r\left[n\right] - \mathbf{w}_b^r\left[n\right]\right)\left(\mathbf{w}_b\left[n\right] - \mathbf{w}_b^r\left[n\right]\right)^T.
\end{aligned}
\tag{32}
$$

The constraint (31) can be reformulated as

$$
0 < \Upsilon\left[n\right] \le \psi\left(\Upsilon\left[n\right]\right), \forall n. \tag{33}
$$

Note that the first term $\hat{R}_k^s\left[n\right]$ in (30) is also non-convex. To this end, let $\psi\left(\hat{R}_k^s\left[n\right]\right)$ be the first order Taylor expansion of $\hat{R}_k^s\left[n\right]$ at any feasible points $\left\|\mathbf{w}_u^r\left[n\right] - \mathbf{w}_b^r\left[n\right]\right\|^2$ and $\left\|\mathbf{q}_b^r\left[n\right] - \mathbf{w}_{bk}\right\|^2 + H_b^r[n]^2$ in the rth iteration, which is given in (34), as shown at the bottom of the page, where

$$
\Omega_{k,1}\left[n\right] = \frac{\frac{\beta_0 p^u[n]}{\left\|\mathbf{w}_u^r[n] - \mathbf{w}_b^r[n]\right\|^4}\log_2 e}{\frac{\beta_0 p^u[n]}{\left\|\mathbf{w}_u^r[n] - \mathbf{w}_b^r[n]\right\|^2} + \frac{\beta_0 p_k^s[n]}{\left\|\mathbf{q}_b^r[n] - \mathbf{w}_{bk}\right\|^2 + H_b^r[n]^2} + \sigma^2}, \tag{35}
$$

and

$$
\Omega_{k,2}\left[n\right] = \frac{\frac{\beta_0 p_k^s[n]}{\left(\left\|\mathbf{q}_b^r[n] - \mathbf{w}_{bk}\right\|^2 + H_b^r[n]^2\right)^2}\log_2 e}{\frac{\beta_0 p^u[n]}{\left\|\mathbf{w}_u^r[n] - \mathbf{w}_b^r[n]\right\|^2} + \frac{\beta_0 p_k^s[n]}{\left\|\mathbf{q}_b^r[n] - \mathbf{w}_{bk}\right\|^2 + H_b^r[n]^2} + \sigma^2}. \tag{36}
$$

In addition, the constraint (15k) is non-convex. With (32), constraint (15k) can be replaced by

$$
\psi\left(\Upsilon\left[n\right]\right) \ge d_{\min}^2, \forall n. \tag{37}
$$

As a result, with (27) and (34), define the following optimization problem

$$
\begin{aligned}
\max_{Q,\Upsilon[n]} \; &\beta_1 \sum_{n=1}^N \sum_{k=1}^K y_k\left[n\right] \\
&\times \left(\psi\left(\hat{R}_k^s\left[n\right]\right) - \log\left(\frac{\beta_0 p^u\left[n\right]}{\Upsilon\left[n\right]} + \sigma^2\right)\right) \\
&+ \beta_2 \sum_{n=1}^N \sum_{l=1}^L x_l[n]\psi\left(R_l^u\left[n\right]\right)
\end{aligned}
\tag{38a}
$$
$$
\text{s.t. } (15f)\text{-}(15j), (33), (37). \tag{38b}
$$

Problem (38) can be efficiently solved by standard methods due to its convexity. Then, a locally optimal solution to problem (26) can be guaranteed by successively updating the 3D UAV trajectory obtained from problem (38).

C. Transmit Power Optimization With Fixed Communication Scheduling and 3D UAV Trajectory

For any given A and Q, the transmit power optimization problem is simplified as

$$
\begin{aligned}
\max_P \; &\beta_1 \sum_{n=1}^N \sum_{k=1}^K y_k\left[n\right]\log_2\left(1 + \frac{h_k\left[n\right] p_k^s\left[n\right]}{f\left[n\right] p^u\left[n\right] + \sigma^2}\right) \\
&+ \beta_2 \sum_{n=1}^N \sum_{l=1}^L x_l[n]\log_2\left(1 + \frac{g_l[n] p^u\left[n\right]}{\sum_{k=1}^K \tilde{h}_{k,l} y_k\left[n\right] p_k^s\left[n\right] + \sigma^2}\right)
\end{aligned}
\tag{39a}
$$
$$
\text{s.t. } (15d), (15e). \tag{39b}
$$

$$
\begin{aligned}
\psi\left(\hat{R}_k^s\left[n\right]\right) = \log\Bigg(&\frac{\beta_0 p^u\left[n\right]}{\left\|\mathbf{w}_u^r\left[n\right] - \mathbf{w}_b^r\left[n\right]\right\|^2} + \frac{\beta_0 p_k^s\left[n\right]}{\left\|\mathbf{q}_b^r\left[n\right] - \mathbf{w}_{bk}\right\|^2 + H_b^r[n]^2} + \sigma^2\Bigg) \\
&- \Omega_{k,1}\left[n\right]\left(\left\|\mathbf{w}_u\left[n\right] - \mathbf{w}_b\left[n\right]\right\|^2 - \left\|\mathbf{w}_u^r\left[n\right] - \mathbf{w}_b^r\left[n\right]\right\|^2\right) \\
&- \Omega_{k,2}\left[n\right]\left(\left\|\mathbf{q}_b\left[n\right] - \mathbf{w}_{bk}\right\|^2 + H_b[n]^2 - \left\|\mathbf{q}_b^r\left[n\right] - \mathbf{w}_{bk}\right\|^2 - H_b^r[n]^2\right)
\end{aligned}
\tag{34}
$$

The objective function (39a) is non-convex. To tackle it, we again apply the SCA method. Specifically, we rewrite $R_k^s[n]$ as

$$R_k^s[n] = \log_2\left(h_k[n]\,p_k^s[n] + f[n]\,p^u[n] + \sigma^2\right) - \tilde{R}_k^s[n], \tag{40}$$

where

$$\tilde{R}_k^s[n] = \log_2\left(f[n]\,p^u[n] + \sigma^2\right). \tag{41}$$

Obviously, (40) is a difference of convex (DC) function. We replace the term $\tilde{R}_k^s[n]$ by its first order Taylor expansion at any given feasible point $p^{u,r}[n]$, denoted as $\psi\left(\tilde{R}_k^s[n]\right)$, and given by

$$\psi\left(\tilde{R}_k^s[n]\right) = \log_2\left(f[n]\,p^{u,r}[n] + \sigma^2\right)$$
$$+ \frac{f[n]\log_2 e}{f[n]\,p^{u,r}[n] + \sigma^2}\left(p^u[n] - p^{u,r}[n]\right). \tag{42}$$

Next, we tackle the non-convexity of $R_l^u[n]$ in (39a) by rewriting $R_l^u[n]$ as

$$R_l^u[n] = \log_2\left(g_l[n]p^u[n] + \sum_{k=1}^K \tilde{h}_{k,l}y_k[n]\,p_k^s[n] + \sigma^2\right)$$
$$- \tilde{R}_l^u[n], \tag{43}$$

where

$$\tilde{R}_l^u[n] = \log_2\left(\sum_{k=1}^K \tilde{h}_{k,l}y_k[n]\,p_k^s[n] + \sigma^2\right). \tag{44}$$

Interestingly, (43) is also a difference of convex (DC) functions. By taking the same steps as in (40), an upper bound for $\tilde{R}_l^u[n]$ at any feasible point $p_k^{s,r}[n]$ is given by

$$\psi\left(\tilde{R}_l^u[n]\right) = \log_2\left(\sum_{k=1}^K \tilde{h}_{k,l}y_k[n]\,p_k^{s,r}[n] + \sigma^2\right)$$
$$+ \sum_{k=1}^K \frac{\tilde{h}_{k,l}y_k[n]}{\sum_{k=1}^K \tilde{h}_{k,l}y_k[n]\,p_k^{s,r}[n] + \sigma^2}$$
$$\times \left(p_k^s[n] - p_k^{s,r}[n]\right). \tag{45}$$

Consequently, with (42) and (45), we define the optimization problem in (46), as shown at the bottom of the page. It can be verified that problem (46) is a convex optimization problem, which can be readily solved. Then, a locally optimal solution to problem (39) can be guaranteed by successively updating the transmit power obtained from problem (46).

Algorithm 3 BCD for Problem (15)

1: **Initialize** P^r, Q^r, and set $r = 0$ as well as tolerance $\epsilon = 10^{-2}$.
2: **repeat**
3:     Solve (25) for given P^r and Q^r, and denoted the optimal solution as A^{r+1}.
4:     Solve (38) for given A^{r+1} and P^r, and denoted the optimal solution as Q^{r+1}.
5:     Solve (46) for given A^{r+1} and Q^{r+1}, and denoted the optimal solution as P^{r+1}.
6:     $r = r + 1$.
7: **until** the fractional increase of the objective value of (15) is smaller than ϵ.

D. Overall Algorithm

Based on the solutions to the three sub-problems above, we alternately optimize the three sub-problems based on the block coordinate descent (BCD) method [24], [29], [47]. The details of the BCD are summarized in Algorithm 3.

The convergence of Algorithm 3 is proved as follows: To facilitate the design, we define $A^{r+1} = \{x_l^r[n], y_k^r[n], \forall l, k, n\}$, $P^r = \{p^{u,r}[n], p_k^{s,r}[n], \forall k, n\}$, and $Q^r = \{\mathbf{w}_u^r[n], \mathbf{w}_b^r[n], \forall n\}$ in the rth iteration. Let $R\left(A^r, Q^r, P^r\right)$, $R_u^{lb}\left(A^r, Q^r, P^r\right)$, $R_q^{lb}\left(A^r, Q^r, P^r\right)$, and $R_p^{lb}\left(A^r, Q^r, P^r\right)$ be the objective value to the relaxed problem (15), (25), (38), and (46) in the $(r+1)$th iteration, respectively. In the rth iteration, in step 3 of Algorithm 3, we have

$$R\left(A^r, Q^r, P^r\right) \stackrel{(a)}{=} R_u^{lb}\left(A^r, Q^r, P^r\right) \stackrel{(b)}{\leq} R_u^{lb}\left(A^{r+1}, Q^r, P^r\right)$$
$$\stackrel{(c)}{\leq} R\left(A^{r+1}, Q^r, P^r\right), \tag{47}$$

where (a) holds since the first-order Taylor expansion in (24) is tight at the given local point A^r, which indicates that problem (25) at A^r has the same objective value as that of problem (23); (b) holds since in step 3 with the given Q^r and P^r, problem (25) is solved optimally with solution A^{r+1}; and (c) holds due to that the objective value of (25) is served as a lower bound to that of (23). The inequality (47) shows that the objective value of (23) is non-decreasing after each iteration. Similar to step 4 and step 5, we respectively have

$$R\left(A^{r+1}, Q^r, P^r\right) = R_q^{lb}\left(A^{r+1}, Q^r, P^r\right)$$
$$\leq R_q^{lb}\left(A^{r+1}, Q^{r+1}, P^r\right)$$
$$\leq R\left(A^{r+1}, Q^{r+1}, P^r\right), \tag{48}$$

$$\max_P \beta_1 \sum_{n=1}^N \sum_{k=1}^K y_k[n]\left(\log_2\left(h_k[n]\,p_k^s[n] + f[n]\,p^u[n] + \sigma^2\right) - \psi\left(\tilde{R}_k^s[n]\right)\right)$$
$$+ \beta_2 \sum_{n=1}^N \sum_{l=1}^L x_l[n]\left(\log_2\left(g_l[n]p^u[n] + \sum_{k=1}^K \tilde{h}_{k,l}y_k[n]\,p_k^s[n] + \sigma^2\right) - \psi\left(\tilde{R}_l^u[n]\right)\right) \tag{46a}$$
$$\text{s.t. } (15d), (15e). \tag{46b}$$

and

$$R\left(A^{r+1}, Q^{r+1}, P^r\right) = R_p^{lb}\left(A^{r+1}, Q^{r+1}, P^r\right)$$
$$\leq R_p^{lb}\left(A^{r+1}, Q^{r+1}, P^{r+1}\right)$$
$$\leq R\left(A^{r+1}, Q^{r+1}, P^{r+1}\right). \quad (49)$$

Based on (47)-(49), we obtain the following inequality

$$R\left(A^r, Q^r, P^r\right) \leq R\left(A^{r+1}, Q^{r+1}, P^{r+1}\right), \quad (50)$$

which shows that the objective value of the relaxed problem (15) is non-decreasing after each iteration. In addition, the maximum objective value of problem (15) is upper bounded by a finite value due to the limited flying time and UAV-AP/SN transmit power budget in practice. Therefore, Algorithm 3 is guaranteed to converge to a locally optimal solution. Note that Algorithm 3 solves the relaxed problem (15), where the binary communication scheduling is relaxed to the continuous variables between 0 and 1. To reconstruct the binary communication scheduling, we directly apply the rounding operation adopted in [30], [31].

Next, we analyze the complexity of Algorithm 3. In step 3 of Algorithm 3, sub-problem (25) is a linear optimization problem, which can be solved by the interior point method with computational complexity $\mathcal{O}\left(L_1\sqrt{KN + LN}\right)$ [48], where $KN + LN$ denotes the total number of variables, and L_1 denotes the number of iterations required to update the communication scheduling. In step 4, since sub-problem (38) involves the logarithmic form, the complexity for solving (38) by using the interior point method is $\mathcal{O}\left(L_2(7N)^{3.5}\right)$ [6], where $7N$ represents the total number of variables, and L_2 denotes the number of iterations required to update the UAV trajectory. Similarly, sub-problem (46) also involves the logarithmic form, the complexity is $\mathcal{O}\left(L_3\left(KN + N\right)^{3.5}\right)$, where L_3 represents the number of iterations required to update the transmit power, and $KN + N$ stands for the number of variables. Therefore, the overall complexity of Algorithm 3 is $\mathcal{O}\left(L_4\left(L_1\left(\sqrt{KN + LN}\right) + L_2(7N)^{3.5} + L_3\left(KN+N\right)^{3.5}\right)\right)$ with L_4 being the number of iterations required by Algorithm 3 to converge.

V. NUMERICAL RESULTS

In this section, numerical examples are provided to validate the effectiveness of the proposed algorithms. Unless otherwise specified, the simulation parameters are set as follows. We assume that the system bandwidth is B=1MHz with noise power $\sigma^2 = -110$dBm [26]. The G2G channel gain is $\beta_0 = -60$dBm with path loss exponent $\alpha = 3$ [38]. The UAV altitude constraints are $H_{\min}$=100m and $H_{\max}$=600m. The maximum horizontal and vertical UAV speed are set to V_{xy}=50m/s and V_z=30m/s, respectively. The minimum safety distance between two UAVs is $d_{\min}$=10m. The maximum UAV-AP and SN transmit power is set as $p_{\max}^s$=0.1W and $p_{\max}^u$=0.1W, respectively. In addition, the duration of each time slot is set as δ=0.5s, and the penalty factor is set as $M = 1 \times 10^5$.
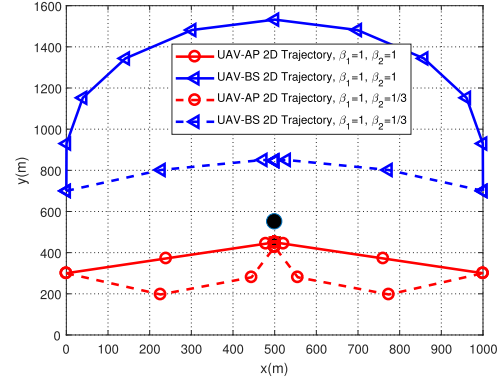

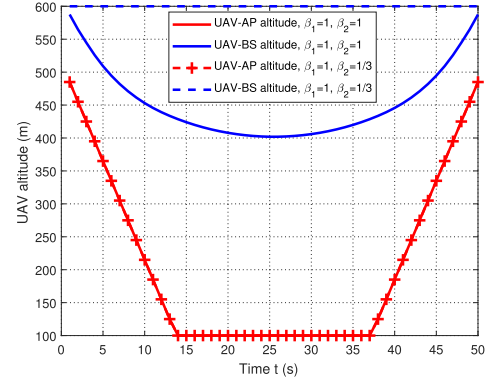Fig. 3. Optimized horizontal UAV trajectories.

Fig. 4. Optimized UAV altitudes.

A. Single SN and Single AP Case

We first consider a simple case where the UAV-BS collects data from one SN, and the UAV-AP transmits its data to one AP. The initial locations of UAVs and AP/SN are set as follows: $\mathbf{q}_{I_u}$=[0 300m], $\mathbf{q}_{I_b}$=[0 700m], $\mathbf{q}_{F_u}$=[1000m 300m], $\mathbf{q}_{F_b}$=[1000m 700m], $\mathbf{w}_{b1}$=[500m 550m], $\mathbf{w}_{u1}$=[500m 450m], H_b=600m, and H_u=500m.

In Fig. 3 and Fig. 4, we plot the UAV-BS and UAV-AP 3D trajectories obtained by the SCA method for different weighting factors β_2=1 and β_2=1/3 when $T = 50s$. In Fig. 3, it is observed that both UAVs remain separated from each other to alleviate the interference received by the UAV-BS from the UAV-AP. In addition, as β_2 becomes smaller, the UAV-BS prefers moving closer to the SN, since the UAV-BS system throughput can be significantly improved by establishing a better channel between the UAV-BS and the SN. In addition, the UAV-AP tends to move far from the UAV-BS to reduce the interference imposed on the UAV-BS-based network. Finally, we can observe from Fig. 4 that under $\beta_1 = 1$ and $\beta_2 = 1$, both UAVs descend to reduce the path loss and improve the system throughput.

In Fig. 5, we investigate the total system throughput versus period T under $\beta_1 = 1$ and $\beta_2 = 1/3$ for different benchmarks to show the superiority of our proposed scheme. The definitions of the abbreviations of the benchmarks are given as below: 1) "3D traj & power": This is our proposed scheme that jointly optimizes the 3D UAV trajectory and communication design; 2) "3D traj & no power": The 3D UAV trajectory and communication scheduling are jointly optimized, but the
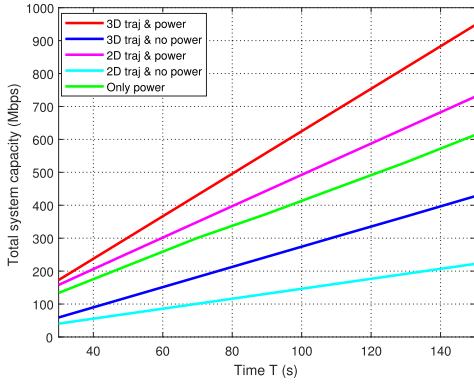
Fig. 5.   System throughput versus period time T.

Fig. 7.   Convergence behavior of Algorithm 3.
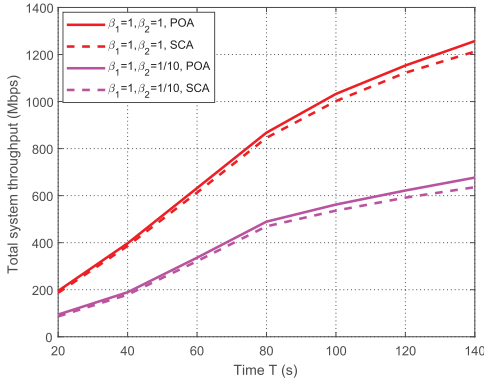
Fig. 6.   Total system throughput versus period T for different weighting factors using POA and SCA methods.

Fig. 8.   Average communication throughput based on approximation versus numerical simulations.

transmit power is fixed at maximum power $p_{\max}^s = p_{\max}^u = 0.1\text{W}$; 3) "2D traj & power": The UAV altitude is fixed, the horizontal UAV trajectory and communication design are jointly optimized; 4) "2D traj & no power": The 2D UAV trajectory and communication scheduling are jointly optimized, but the transmit power of the UAV/SN and altitude of the UAV are fixed ($p_{\max}^s = p_{\max}^u = 0.1\text{W}$); 5) "Only power": The UAV horizontal trajectory and altitude are predetermined, the horizontal trajectory for the UAV-AP/UAV-BS is a straight line from its initial location to its final location with constant speed). However, the communication design, including communication scheduling and transmit power, is optimized. First, we observe that our proposed scheme is superior to the other benchmarks and achieves significant throughput gains, especially when the period becomes larger. Second, the system throughput can be improved by controlling the UAV altitude. For instance, for period $T = 130s$, the system throughput for the proposed scheme is 818Mbps, and for the "2D trajectory & power" method is 634Mbps, which provides a nearly 23% increase. In addition, the system throughput can be significantly improved by controlling the transmit power. For example, for period $T = 130s$, the system throughput for the "3D trajectory & no power" method is 365Mbps, and for the "2D trajectory & no power" method is 191Mbps, which correspond to a 55% and 76% increase in the system throughput, respectively. Finally, the UAV trajectory design also has significantly impacts on the system performance. For example, for period $T = 130s$, the system throughput for the "only power" method is 530Mbps, which results in a 35%
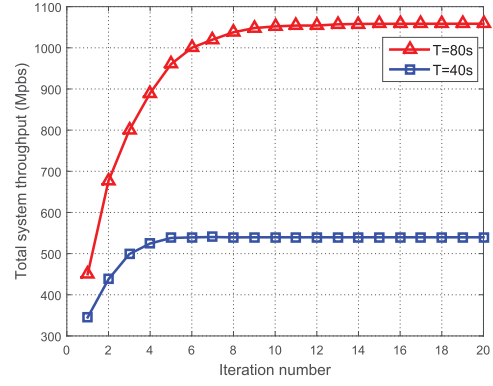
increase in the system throughput compared with our proposed method.

B. Multiple SNs and Multiple APs Case

In this section, we consider a more practical case where the UAV-BS and UAV-AP simultaneously serve multiple SNs and APs. The communication design, including power control and communication scheduling, and UAV trajectory are optimized. We consider 4 SNs and 4 APs, which are respectively located at $\mathbf{w}_{b1}=[-1000\text{m}\ 0]$, $\mathbf{w}_{b2}=[-100\text{m}\ 700\text{m}]$, $\mathbf{w}_{b3}=[0\ 0]$, $\mathbf{w}_{b4}=[-500\text{m}\ -500\text{m}]$, $\mathbf{w}_{u1}=[1000\text{m}\ 0]$, $\mathbf{w}_{u2}=[0\ 700\text{m}]$, $\mathbf{w}_{u3}=[100\text{m}\ 0]$, $\mathbf{w}_{u4}=[700\text{m}\ -400\text{m}]$.

In Fig. 6, we compare the total sum system throughput achieved by the POA and SCA method, versus period T, for different weighting factors. The initial trajectories for the UAV-BS and UAV-AP are circles with given radii and centers. Specifically, for any given period T and maximum UAV horizontal speed V_{xy}, the circle radius is first calculated by $r_c = \frac{V_{xy}T}{2\pi}, c \in \{b, u\}$. Second, for any given location of $\mathbf{w}_{ci}, c \in \{b, u\}, i \in \{\mathcal{K}, \mathcal{L}\}$, the geometric center of the SNs and APs are $\mathbf{ge}_b = \frac{\sum_{i=1}^{K} \mathbf{w}_{bi}}{K} = [x_b\ y_b]$ and $\mathbf{ge}_u = \frac{\sum_{i=1}^{L} \mathbf{w}_{ui}}{L} = [x_u\ y_u]$, respectively. Here, we consider two different weighting factors: $\beta_1 = 1, \beta_2 = 1$ and $\beta_1 = 1, \beta_2 = 1/10$. As can be seen, when period T is small, namely $T \leq 80s$, the system throughput obtained by the POA-based and SCA-based method is nearly the same both for the two different weighting factors. Even as T becomes larger, the throughput gap between
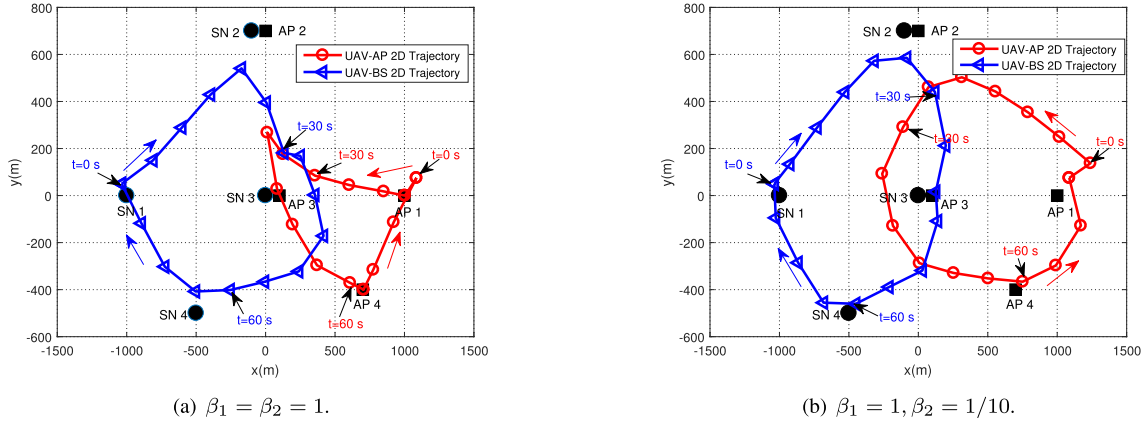
Fig. 9. UAV trajectories for different weighting factors under $T = 80s$. Each trajectory is sampled every 5 seconds with the blue left arrow $\triangleleft$ marking the UAV-BS trajectory and the red circle o marking the UAV-AP trajectory.

the two algorithms still remains quite small. In addition, for $T = 80s$ under $\beta_1 = 1, \beta_2 = 1/10$, the running time for the SCA-based method is about 3.7 minutes, while for the POA-based method is nearly 27 hours. This indicates that the SCA based method can achieve nearly the same optimal performance of the POA-based method while with much lower computational complexity.

In Fig. 7, we show the convergence behavior of Algorithm 3 for different periods T, namely $T = 80s$ and $T = 40s$, under $\beta_1 = \beta_2 = 1$. It is observed that the system throughput obtained by the different periods T all increases quickly with the number of iterations. For a small period $T = 40s$, the proposed algorithm converges in about 6 iterations, while for a large period $T = 80s$, only 10 iterations is required for achieving convergence, which demonstrates the efficiency of Algorithm 3.

In order to evaluate the accuracy of the approximation of the expected throughput both for uplink and downlink, i.e., $R_k^s[n]$ and $R_u^l[n]$, $\forall k, l, n$, developed in (13) and (14), the average throughput based on $R_k^s[n] = \mathbb{E}\{\bar{R}_k^s[n]\}$ and $R_l^u[n] = \mathbb{E}\{\bar{R}_l^u[n]\}$ obtained via numerical simulations is compared. Fig. 8 shows the results of approximation and numerical simulations under Rician factors $K_a = K_s = K_u = 3$dB, $T = 80s$, and $\beta_1 = \beta_2 = 1$. Since there are multiple SNs and APs, we pick one SN and one AP, and compare the results of $R_1^s[n]$ and $R_1^u[n]$ without loss of generality. In addition, for the numerical simulation of the average throughput, the UAV trajectory and UAV-AP/SN transmit power are set as that obtained via Algorithm 3, and the average throughput is taken over 10^4 random channel generations at each time slot. It is observed that the approximation results match well with the simulation results for both SN's throughput and AP's throughput at any time slot. In addition, the upper bound and lower bound of the average throughput obtained via numerical simulations are also plotted. One can see that the obtained approximation results indeed lie in the interval between them, which are consistent with (52) and (54) in Appendix A. It should be noted that the curves of lower bound results are not smooth, and fluctuate drastically in some time slots. This is because in some time slots, the numerator in the logarithm form approaches nearly zero (See X in the left hand side of (52) and (54)).

In the following, the 3D UAV trajectory, speed, transmit power, and system throughput are evaluated under different weighting factors: $\beta_1 = \beta_2 = 1$, and $\beta_1 = 1, \beta_2 = 1/10$. In Fig. 9, we show the optimized UAV trajectories obtained from Algorithm 3 under different weighting factors. It can be observed from Fig. 9 (a) that both UAVs, i.e., UAV-BS and UAV-AP, sequentially visit SNs and APs, respectively. This is because that the path loss between the UAV and the ground node would be significantly reduced as the UAV moves closer to the ground node, thereby improving the system throughput. One can also see the trajectory that UAV flies from one ground node to another ground node is not a straight line. The reasons have two aspects. One the one hand, the AP not only receives the desired signal from the UAV-AP, but also suffers from interference from the SNs. On the other hand, the UAV-BS not only collects desired data from the SNs, but also encounters interference from the UAV-AP. Therefore, the two UAVs trajectories need to be carefully designed so as to mitigate the strong interference. For $\beta_1 = 1, \beta_2 = 1/10$ in Fig. 9 (b), we can obtain the similar trajectories as the case of $\beta_1 = \beta_2 = 1$. However, we can observe from Fig. 9 (b) that the trajectory that UAV-BS flies from one ground node to another ground node is nearly straight. This is because the UAV-BS networks has a high priority over the UAV-AP networks when $\beta_1 > \beta_2$. Therefore, the UAV-BS tends to maximize its own network throughput by optimizing the UAV-BS trajectory. Moreover, the corresponding UAV altitude for the different weighting factors is plotted in Fig. 10. It can be observed that both UAVs descend to reduce the path loss, thereby improving the system throughput. This also indicates that the UAV altitude provides an additional degree of freedom for performance enhancement.

In Fig. 11, the UAV speed for the different weighting factors under $T = 80s$ is plotted. It is observed from Fig. 11 (a) that the UAV flies either with nearly maximum horizontal speed or zero. This is because exploiting the UAV altitude provides an additional degree of freedom for performance enhancement. Unlink Fig. 11 (a), the UAV-AP flies with the maximum horizontal UAV speed for nearly the whole period T in Fig. 11 (b). This is because that the weighting factor $\beta_2 = 1/10$ for the UAV-AP networks is small.
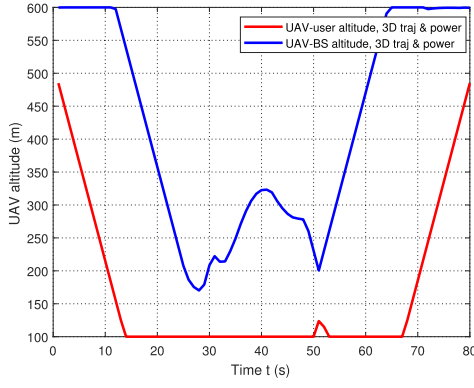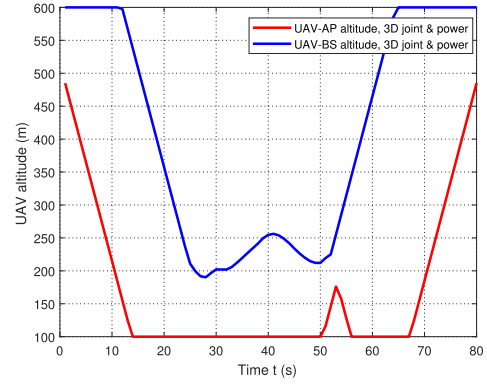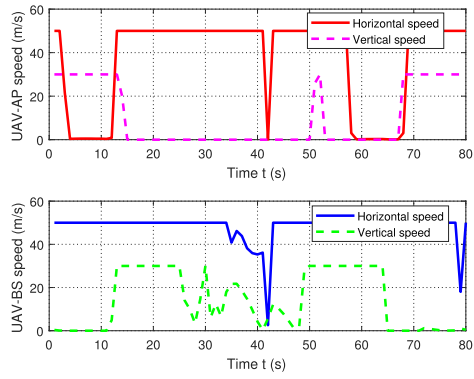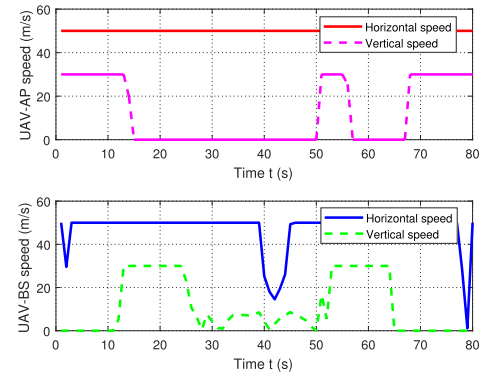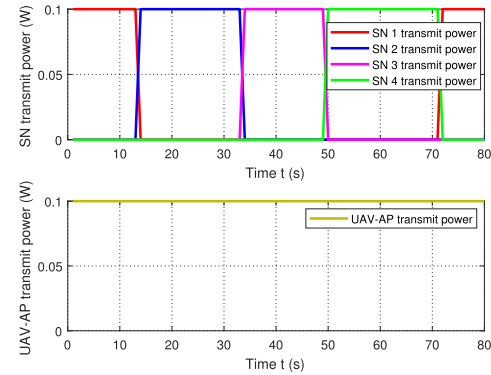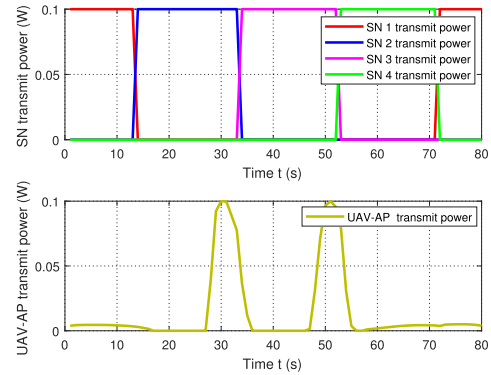
(a) $\beta_1 = \beta_2 = 1$.

(b) $\beta_1 = 1, \beta_2 = 1/10$.

Fig. 10.   Optimized UAV altitudes for the different weight factors under $T = 80s$.

(a) $\beta_1 = 1, \beta_2 = 1$.

(b) $\beta_1 = 1, \beta_2 = 1/10$.

Fig. 11.   Optimized UAV speed for the different weight factors under $T = 80s$.

(a) $\beta_1 = 1, \beta_2 = 1$.

(b) $\beta_1 = 1, \beta_2 = 1/10$.

Fig. 12.   Optimized UAV-AP/SN transmit power for the different weight factors under $T = 80s$.

Fig. 12 shows the UAV-AP/SN transmit power for the different weighting factors under $T = 80s$ It can be seen from Fig. 12 (a) that the UAV-AP always transmits with maximum power, and the SNs transmit either with maximum power or zero. However, in Fig. 12 (b), the UAV-AP transmits with maximum power only from $t = 28s$ to $t = 35s$ and $t = 48s$ to $t = 55s$, and no power is transmitted during other times. This is expected since with a smaller β_2, the UAV-AP keeps mute will alleviate the interference imposed on the UAV-BS, thereby improving the UAV-BS system throughput.

In Fig. 13, we compare our proposed design with different benchmarks for the different weighting factors in terms of system throughput. The UAV-AP, UAV-BS, and the total system throughput are respectively shown in Fig. 13 (a), Fig. 13 (b), and Fig. 13 (c). First, we see that our proposed scheme significantly outperforms the other benchmarks as shown in Fig. 13 (c). For example, for period $T = 120s$ and $\beta_2 = 1$, the total system throughput for the proposed scheme is 1551Mbps, which is 30% higher than for "3D traj & no power" (1074 Mbps), 20% higher than "2D
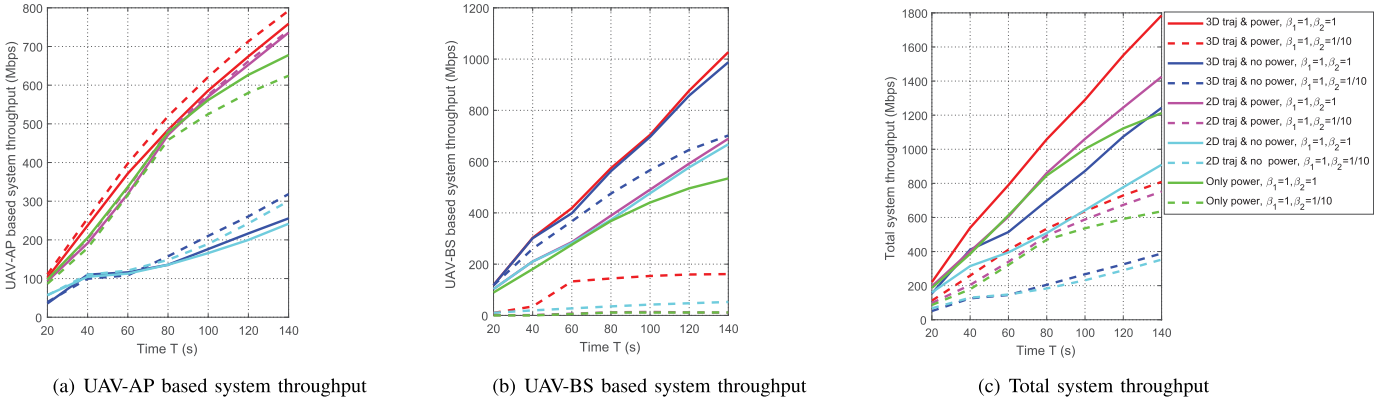
(a) UAV-AP based system throughput   (b) UAV-BS based system throughput   (c) Total system throughput

Fig. 13. System throughput versus period T for different benchmarks under different weighting factors.

traj & power" (1245 Mbps), 50% higher than "2D traj & no power" (777 Mbps), and 27% higher than the "only power" (1122 Mbps) algorithm. This demonstrates the superiority of the proposed scheme. In addition, the benefits of system performance gains can be obtained via UAV altitude optimization, which again confirms that 3D trajectory optimization outperforms 2D trajectory optimization. Second, we can observe from Fig. 13 (b) that "3D traj & power" with $\beta_1 = \beta_2 = 1$ achieves a higher system throughput than "3D traj & power" with $\beta_1 = 1, \beta_2 = 1/10$. This is because the UAV-BS network has a high priority compared to the UAV-AP network when $\beta_1 > \beta_2$, thereby significantly improving the UAV-BS system throughput.

VI. CONCLUSION

This paper studied the UAV-aided simultaneous uplink and downlink transmission networks, where one UAV-AP migrated data to the APs, and one UAV-BS collected data from the SNs. First, we considered a scenario where the two UAV trajectories were pre-determined, and the system throughput was maximized by leveraging the polyblock outer approximation method. Second, we developed a 3D trajectory and communication design approach for maximizing the system throughput, and a locally optimal solution was achieved by applying the successive convex approximation method. Numerical results showed that the proposed successive convex approximation method achieved nearly the same system throughput compared with the polyblock outer approximation method when the UAVs trajectory were pre-determined. In addition, compared with the benchmarks, a significant system throughput gain was obtained by optimizing the 3D UAV trajectory as well as the transmit power. This work can be extended by considering multiple UAV-BS and UAV-AP. The additional interference caused by additional UAV-BS and UAV-AP should be carefully managed in order to maximize the system throughput.

APPENDIX A
PROOF OF THEOREM 1

Let $f_1(z) = \log_2(1 + z)$ and $f_2(z) = \log_2\left(1 + \frac{1}{z}\right)$, $z > 0$. It can be readily checked that $f_1(z)$ is concave with respect to z and $f_2(z)$ is convex with respect to z, based on the Jensen's inequality [46], which thus leads to the following

inequalities

$$\log_2\left(1 + \frac{1}{\mathbb{E}\left\{\frac{1}{z}\right\}}\right) \leq \mathbb{E}\left\{\log_2(1+z)\right\} \leq \log_2(1 + \mathbb{E}\{z\}). \tag{51}$$

Define $z = \frac{X}{Y}$ $(X > 0, Y > 0)$, we have

$$\log_2\left(1 + \frac{1}{\mathbb{E}\left\{\frac{Y}{X}\right\}}\right) \leq \mathbb{E}\left\{\log_2\left(1 + \frac{X}{Y}\right)\right\}$$
$$\leq \log_2\left(1 + \mathbb{E}\left\{\frac{X}{Y}\right\}\right). \tag{52}$$

If X and Y are independent with each other $(X > 0$ and $Y > 0)$, we have

$$\mathbb{E}\left\{\frac{X}{Y}\right\} = \mathbb{E}\{X\}\mathbb{E}\left\{\frac{1}{Y}\right\} \geq \frac{\mathbb{E}\{X\}}{\mathbb{E}\{Y\}}, \tag{53}$$

where the inequality holds due to the convexity of function $\frac{1}{Y}$ for $Y > 0$ and Jensen's inequality. Based on (53), we can derive

$$\log_2\left(1 + \frac{1}{\mathbb{E}\left\{\frac{Y}{X}\right\}}\right) \leq \log_2\left(1 + \frac{\mathbb{E}\{X\}}{\mathbb{E}\{Y\}}\right)$$
$$\leq \log_2\left(1 + \mathbb{E}\left\{\frac{X}{Y}\right\}\right). \tag{54}$$

Comparing (52) and (54), we can see that $\mathbb{E}\left\{\log_2\left(1 + \frac{X}{Y}\right)\right\}$ and $\log_2\left(1 + \frac{\mathbb{E}\{X\}}{\mathbb{E}\{Y\}}\right)$ have the same lower bound and upper bound results. In addition, for the special case $X = 0, Y > 0$, we have $\mathbb{E}\left\{\log_2\left(1 + \frac{X}{Y}\right)\right\} = \log_2\left(1 + \frac{\mathbb{E}\{X\}}{\mathbb{E}\{Y\}}\right) = 0$. As a result, we obtain the approximation results in (12).

APPENDIX B
PROOF OF THEOREM 2

We prove Theorem 2 in two steps. In the first step, we show that the optimal SN transmit power (UAV-AP transmit power) for problem (17) results in at most one SN (AP) being active in each time slot. Define $\check{R}_k^s[n]$ as

$$\check{R}_k^s[n]$$
$$= \log_2\left(1 + \frac{h_k[n]\tilde{p}_k^s[n]}{M\sum_{i \neq k}^{K}\tilde{p}_i^s[n] + \sum_{l=1}^{L}f[n]\tilde{p}_l^u[n] + \sigma^2}\right). \tag{55}$$

Suppose that more than one SN is active, and assume that there is K_1 number of SNs whose transmit power are non-zero, define $\tilde{p}_k^s[n] \neq 0$ for $k = 1, \ldots, K_1$ ($2 \leq K_1 \leq K$) and $\tilde{p}_k^s[n] = 0$ for $k = K_1 + 1, \ldots, K$. Obviously, for $\forall k \in \{K_1 + 1, \ldots, K\}$, $\check{R}_k^s[n] = 0$. For $\forall k \in \{1, \ldots, K_1\}$ with a sufficiently large penalty factor $M \gg 1$, $M \sum_{i \neq k}^{K} \tilde{p}_i^s[n] \to \infty$. Thus, $\sum_{k=1}^{K} \check{R}_k^s[n] = 0$ at any time slot n. Suppose that there is only one SN whose transmit power is non-zero. We assume that $\tilde{p}_1^s[n] \neq 0$ and $\tilde{p}_k^s[n] = 0$ for $k = 2, \ldots, K$. We have

$$
\sum_{k=1}^{K} R_k^s[n] = \log_2\left(1 + \frac{h_1[n]\tilde{p}_1^s[n]}{\sum_{l=1}^{L} f[n]\tilde{p}_l^u[n] + \sigma^2}\right)
$$
$$
\overset{a}{=} \log_2\left(1 + \frac{h_1[n]\tilde{p}_1^s[n]}{f[n]\tilde{p}_l^u[n] + \sigma^2}\right) > 0, \quad (56)
$$

where (a) holds since at most one AP is scheduled at any time slot n shown in the later (we assume that AP l is scheduled here without loss of generality). Therefore, we can declare that at most one SN is active in order to maximize (17). Similarly, define

$$
\check{R}_l^u[n]
$$
$$
= \log_2\left(1 + \frac{g_l[n]\tilde{p}_l^u[n]}{M\sum_{i \neq l}^{L} \tilde{p}_i^u[n] + \sum_{k=1}^{K} \tilde{h}_{k,l}\tilde{p}_k^s[n] + \sigma^2}\right).
$$
$$
(57)
$$

It is not difficult to verify that at most one AP can be active in order to maximize (17), based on the same derivation as in (55).

In the second step, we show that (17) is equivalent to (16). First, it can be easily seen that the optimal solution to problem (16) is feasible for problem (17) with the same objective value. Second, based on the first step, we see that the optimal solution to problem (17) is also feasible for problem (16) with same objective value. This thus completes the proof of Theorem 2.

REFERENCES

[1] M. Mozaffari, W. Saad, M. Bennis, Y.-H. Nam, and M. Debbah, "A tutorial on UAVs for wireless networks: Applications, challenges, and open problems," *IEEE Commun. Surveys Tuts.*, vol. 21, no. 3, pp. 2334–2360, 3rd Quart., 2019.

[2] Y. Zeng, R. Zhang, and T. J. Lim, "Wireless communications with unmanned aerial vehicles: Opportunities and challenges," *IEEE Commun. Mag.*, vol. 54, no. 5, pp. 36–42, May 2016.

[3] M. M. Azari, H. Sallouha, A. Chiumento, S. Rajendran, E. Vinogradov, and S. Pollin, "Key technologies and system trade-offs for detection and localization of amateur drones," *IEEE Commun. Mag.*, vol. 56, no. 1, pp. 51–57, Jan. 2018.

[4] F. Jiang and A. L. Swindlehurst, "Optimization of UAV heading for the Ground-to-Air uplink," *IEEE J. Sel. Areas Commun.*, vol. 30, no. 5, pp. 993–1005, Jun. 2012.

[5] Z. Han, A. L. Swindlehurst, and K. Liu, "Optimization of MANET connectivity via smart deployment/movement of unmanned air vehicles," *IEEE Trans. Veh. Technol.*, vol. 58, no. 7, pp. 3533–3546, Sep. 2009.

[6] G. Zhang, Q. Wu, M. Cui, and R. Zhang, "Securing UAV communications via joint trajectory and power control," *IEEE Trans. Wireless Commun.*, vol. 18, no. 2, pp. 1376–1389, Feb. 2019.

[7] Q. Wu and R. Zhang, "Common throughput maximization in UAV-enabled OFDMA systems with delay consideration," *IEEE Trans. Commun.*, vol. 66, no. 12, pp. 6614–6627, Dec. 2018.

[8] Q. Song, F.-C. Zheng, Y. Zeng, and J. Zhang, "Joint beamforming and power allocation for UAV-enabled full-duplex relay," *IEEE Trans. Veh. Technol.*, vol. 68, no. 2, pp. 1657–1671, Feb. 2019.

[9] X. Li, H. Yao, J. Wang, X. Xu, C. Jiang, and L. Hanzo, "A near-optimal UAV-aided radio coverage strategy for dense urban areas," *IEEE Trans. Veh. Technol.*, vol. 68, no. 9, pp. 9098–9109, Sep. 2019.

[10] X. Zhou, Q. Wu, S. Yan, F. Shu, and J. Li, "UAV-enabled secure communications: Joint trajectory and transmit power optimization," *IEEE Trans. Veh. Technol.*, vol. 68, no. 4, pp. 4069–4073, Apr. 2019.

[11] Y. Zeng, Q. Wu, and R. Zhang, "Accessing from the sky: A tutorial on UAV communications for 5G and beyond," *Proc. IEEE*, vol. 107, no. 12, pp. 2327–2375, Dec. 2019.

[12] I. Jawhar, N. Mohamed, J. Al-Jaroodi, and S. Zhang, "A framework for using unmanned aerial vehicles for data collection in linear wireless sensor networks," *J. Intell. Robot. Syst.*, vol. 74, nos. 1–2, pp. 437–453, Apr. 2014.

[13] M. Dong, K. Ota, M. Lin, Z. Tang, S. Du, and H. Zhu, "UAV-assisted data gathering in wireless sensor networks," *J. Supercomput.*, vol. 70, no. 3, pp. 1142–1155, Apr. 2014.

[14] C. Zhan, Y. Zeng, and R. Zhang, "Energy-efficient data collection in UAV enabled wireless sensor network," *IEEE Wireless Commun. Lett.*, vol. 7, no. 3, pp. 328–331, Jun. 2018.

[15] Y. Zeng, J. Lyu, and R. Zhang, "Cellular-connected UAV: Potential, challenges, and promising technologies," *IEEE Wireless Commun.*, vol. 26, no. 1, pp. 120–127, Feb. 2019.

[16] S. Zhang, Y. Zeng, and R. Zhang, "Cellular-enabled UAV communication: A connectivity-constrained trajectory optimization perspective," *IEEE Trans. Commun.*, vol. 67, no. 3, pp. 2580–2604, Mar. 2019.

[17] S. Zhang, H. Zhang, B. Di, and L. Song, "Cellular UAV-to-X communications: Design and optimization for multi-UAV networks," *IEEE Trans. Wireless Commun.*, vol. 18, no. 2, pp. 1346–1359, Feb. 2019.

[18] A. Fotouhi *et al.*, "Survey on UAV cellular communications: Practical aspects, standardization advancements, regulation, and security challenges," *IEEE Commun. Surveys Tuts.*, vol. 21, no. 4, pp. 3417–3442, 4th Quart., 2019.

[19] M. M. Azari, F. Rosas, and S. Pollin, "Cellular connectivity for UAVs: Network modeling, performance analysis, and design guidelines," *IEEE Trans. Wireless Commun.*, vol. 18, no. 7, pp. 3366–3381, Jul. 2019.

[20] M. Alzenad, A. El-Keyi, and H. Yanikomeroglu, "3-D placement of an unmanned aerial vehicle base station for maximum coverage of users with different QoS requirements," *IEEE Wireless Commun. Lett.*, vol. 7, no. 1, pp. 38–41, Feb. 2018.

[21] A. Al-Hourani, S. Kandeepan, and S. Lardner, "Optimal LAP altitude for maximum coverage," *IEEE Wireless Commun. Lett.*, vol. 3, no. 6, pp. 569–572, Dec. 2014.

[22] M. M. Azari, F. Rosas, K.-C. Chen, and S. Pollin, "Ultra reliable UAV communication using altitude and cooperation diversity," *IEEE Trans. Commun.*, vol. 66, no. 1, pp. 330–344, Jan. 2018.

[23] M. Mozaffari, W. Saad, M. Bennis, and M. Debbah, "Efficient deployment of multiple unmanned aerial vehicles for optimal wireless coverage," *IEEE Commun. Lett.*, vol. 20, no. 8, pp. 1647–1650, Aug. 2016.

[24] J. Wang, C. Jiang, Z. Wei, C. Pan, H. Zhang, and Y. Ren, "Joint UAV hovering altitude and power control for Space-Air-Ground IoT networks," *IEEE Internet Things J.*, vol. 6, no. 2, pp. 1741–1753, Apr. 2019.

[25] H. Dai, H. Zhang, M. Hua, C. Li, Y. Huang, and B. Wang, "How to deploy multiple UAVs for providing communication service in an unknown region?" *IEEE Wireless Commun. Lett.*, vol. 8, no. 4, pp. 1276–1279, Aug. 2019.

[26] Y. Zeng and R. Zhang, "Energy-efficient UAV communication with trajectory optimization," *IEEE Trans. Wireless Commun.*, vol. 16, no. 6, pp. 3747–3760, Jun. 2017.

[27] C. You and R. Zhang, "3D trajectory optimization in rician fading for UAV-enabled data harvesting," *IEEE Trans. Wireless Commun.*, vol. 18, no. 6, pp. 3192–3207, Jun. 2019.

[28] Y. Sun, D. Xu, D. W. K. Ng, L. Dai, and R. Schober, "Optimal 3D-trajectory design and resource allocation for solar-powered UAV communication systems," *IEEE Trans. Commun.*, vol. 67, no. 6, pp. 4281–4298, Jun. 2019.

[29] Q. Wu, Y. Zeng, and R. Zhang, "Joint trajectory and communication design for multi-UAV enabled wireless networks," *IEEE Trans. Wireless Commun.*, vol. 17, no. 3, pp. 2109–2121, Mar. 2018.

[30] M. Hua, Y. Wang, Q. Wu, H. Dai, Y. Huang, and L. Yang, "Energy-efficient cooperative secure transmission in multi-UAV-enabled wireless networks," *IEEE Trans. Veh. Technol.*, vol. 68, no. 8, pp. 7761–7775, Aug. 2019.

[31] M. Hua, L. Yang, C. Pan, and A. Nallanathan, "Throughput maximization for full-duplex UAV aided small cell wireless systems," *IEEE Wireless Commun. Lett.*, vol. 9, no. 4, pp. 475–479, Apr. 2020.

[32] A. A. Khuwaja, Y. Chen, N. Zhao, M.-S. Alouini, and P. Dobbins, "A survey of channel modeling for UAV communications," *IEEE Commun. Surveys Tuts.*, vol. 20, no. 4, pp. 2804–2821, 4th Quart., 2018.

[33] C. Zhan and Y. Zeng, "Aerial–ground cost tradeoff for multi-UAV-enabled data collection in wireless sensor networks," *IEEE Trans. Commun.*, vol. 68, no. 3, pp. 1937–1950, Mar. 2020.

[34] M. Mahdi Azari, G. Geraci, A. Garcia-Rodriguez, and S. Pollin, "UAV-to-UAV communications in cellular networks," 2019, *arXiv:1912.07534*. [Online]. Available: http://arxiv.org/abs/1912.07534

[35] N. Ahmed, S. S. Kanhere, and S. Jha, "On the importance of link characterization for aerial wireless sensor networks," *IEEE Commun. Mag.*, vol. 54, no. 5, pp. 52–57, May 2016.

[36] J. Allred, A. B. Hasan, S. Panichsakul, W. Pisano, and K. Mohseni, "Sensorflock: An airborne wireless sensor network of micro-air vehicles," in *Proc. SenSys*, Nov. 2007, pp. 1937–1950.

[37] J. Xu, Y. Zeng, and R. Zhang, "UAV-enabled wireless power transfer: Trajectory design and energy optimization," *IEEE Trans. Wireless Commun.*, vol. 17, no. 8, pp. 5092–5106, Aug. 2018.

[38] J. Lyu, Y. Zeng, and R. Zhang, "UAV-aided offloading for cellular hotspot," *IEEE Trans. Wireless Commun.*, vol. 17, no. 6, pp. 3988–4001, Jun. 2018.

[39] F. Zhou, Y. Wu, R. Q. Hu, and Y. Qian, "Computation rate maximization in UAV-enabled wireless-powered mobile-edge computing systems," *IEEE J. Sel. Areas Commun.*, vol. 36, no. 9, pp. 1927–1941, Sep. 2018.

[40] M. Hua, Y. Wang, Z. Zhang, C. Li, Y. Huang, and L. Yang, "Power-efficient communication in UAV-aided wireless sensor networks," *IEEE Commun. Lett.*, vol. 22, no. 6, pp. 1264–1267, Jun. 2018.

[41] Q. Wu, J. Xu, and R. Zhang, "Capacity characterization of UAV-enabled two-user broadcast channel," *IEEE J. Sel. Areas Commun.*, vol. 36, no. 9, pp. 1955–1971, Sep. 2018.

[42] J. Lyu, Y. Zeng, and R. Zhang, "Cyclical multiple access in UAV-aided communications: A throughput-delay tradeoff," *IEEE Wireless Commun. Lett.*, vol. 5, no. 6, pp. 600–603, Dec. 2016.

[43] H. Tuy, "Monotonic optimization: Problems and solution approaches," *SIAM J. Optim.*, vol. 11, no. 2, pp. 464–494, Jan. 2000.

[44] Y. J. A. Zhang *et al.*, "Monotonic optimization in communication and networking systems," *Found Trends Netw.*, vol. 7, no. 1, pp. 1–75, Oct. 2013.

[45] A. Zappone, E. Bjornson, L. Sanguinetti, and E. Jorswieck, "Globally optimal energy-efficient power control and receiver design in wireless networks," *IEEE Trans. Signal Process.*, vol. 65, no. 11, pp. 2844–2859, Jun. 2017.

[46] S. Boyd and L. Vandenberghe, *Convex optimization*. Cambridge, U.K.: Cambridge Univ. Press, 2004.

[47] H. Wang, J. Wang, G. Ding, J. Chen, Y. Li, and Z. Han, "Spectrum sharing planning for full-duplex UAV relaying systems with underlaid D2D communications," *IEEE J. Sel. Areas Commun.*, vol. 36, no. 9, pp. 1986–1999, Sep. 2018.

[48] J. Gondzio and T. Terlaky, "A computational view of interior point methods," in *Advances in Linear and Integer Programming* (Oxford Lecture Series in Mathematics and its Applications), vol. 4. New York, NY, USA: Oxford Univ. Press, 1996, pp. 103–144.

Luxi Yang (Senior Member, IEEE) received the M.S. and Ph.D. degrees in electrical engineering from Southeast University, Nanjing, China, in 1990 and 1993, respectively. Since 1993, he has been with the Department of Radio Engineering, Southeast University, where he is currently a Full Professor of information systems and communications and the Director of the Digital Signal Processing Division. He has authored or coauthored two published books and more than 200 journal articles. He holds 50 patents. His current research interests include signal processing for wireless communications, MIMO communications, intelligent wireless communications, and statistical signal processing. He is currently a member of Signal Processing Committee of the Chinese Institute of Electronics. He received the first and second class prizes of science and technology progress awards of the State Education Ministry of China in 1998, 2002, and 2014.

Qingqing Wu (Member, IEEE) received the B.Eng. degree from the South China University of Technology in 2012 and the Ph.D. degree from Shanghai Jiao Tong University (SJTU) in 2016, in electronic engineering.

He was a Research Fellow with the Department of Electrical and Computer Engineering, National University of Singapore. He is currently an Assistant Professor with the Department of Electrical and Computer Engineering, University of Macau, China, and also with the State Key Laboratory of Internet of Things for Smart City. He has published more than 60 IEEE journal and conference papers. His current research interest includes intelligent reflecting surface (IRS), unmanned aerial vehicle (UAV) communications, and MIMO transceiver design. He was a recipient of the IEEE WCSP Best Paper Award in 2015, the Outstanding Ph.D. Thesis Funding in SJTU in 2016, and the Outstanding Ph.D. Thesis Award of China Institute of Communications in 2017. He was the Exemplary Editor of IEEE COMMUNICATIONS LETTERS in 2019 and the exemplary reviewer of several IEEE journals. He serves as an Associate Editor for IEEE COMMUNICATIONS LETTERS and IEEE OPEN JOURNAL OF COMMUNICATIONS SOCIETY. He is the Lead Guest Editor of IEEE JOURNAL ON SELECTED AREAS IN COMMUNICATIONS on UAV Communications in 5G and Beyond Networks, and the Guest Editor of IEEE OPEN JOURNAL ON VEHICULAR TECHNOLOGY on 6G Intelligent Communications and IEEE OPEN JOURNAL OF COMMUNICATIONS SOCIETY on Reconfigurable Intelligent Surface-Based Communications for 6G Wireless Networks. He is the workshop Co-Chair of ICC 2019 and ICC 2020 workshop on Integrating UAVs into 5G and Beyond, and the workshop Co-Chair of GLOBECOM 2020 workshop on Reconfigurable Intelligent Surfaces for Wireless Communication for Beyond 5G.

A. Lee Swindlehurst (Fellow, IEEE) received the B.S. and M.S. degrees in electrical engineering from Brigham Young University (BYU), in 1985 and 1986, respectively, and the Ph.D. degree in electrical engineering from Stanford University, in 1991. He was with the Department of Electrical and Computer Engineering, BYU, from 1990 to 2007, where he has served as the Department Chair from 2003 to 2006. From 1996 to 1997, he held a joint appointment as a Visiting Scholar with Uppsala University and the Royal Institute of Technology, Sweden. From 2006 to 2007, he was on leave working as the Vice President of Research for ArrayComm LLC in San Jose, CA, USA. Since 2007, he has been a Professor with the Electrical Engineering and Computer Science Department, University of California Irvine, where he has served as the Associate Dean for Research and Graduate Studies with the Samueli School of Engineering from 2013 to 2016. From 2014 to 2017, he was also a Hans Fischer Senior Fellow with the Institute for Advanced Studies, Technical University of Munich. In 2016, he was elected as a Foreign Member of the Royal Swedish Academy of Engineering Sciences (IVA). His research focuses on array signal processing for radar, wireless communications, and biomedical applications. He has more than 300 publications in these areas. He was the inaugural Editor-in-Chief of IEEE JOURNAL OF SELECTED TOPICS IN SIGNAL PROCESSING. He received the 2000 IEEE W. R. G. Baker Prize Paper Award, the 2006 IEEE Communications Society Stephen O. Rice Prize in the Field of Communication Theory, the 2006 and 2010 IEEE Signal Processing Society's best paper awards, and the 2017 IEEE Signal Processing Society Donald G. Fink Overview Paper Award.

Meng Hua (Student Member, IEEE) received the M.S. degree in electrical and information engineering from the Nanjing University of Science and Technology, Nanjing, China, in 2016. He is currently pursuing the Ph.D. degree with the School of Information Science and Engineering, Southeast University, Nanjing, China. His current research interests include UAV assisted communication, intelligent reflecting surface (IRS), backscatter communication, energy-efficient wireless communication, X-connectivity, cognitive radio network, secure transmission, and optimization theory.